HHS Public Access

Author manuscript

Dev Biol. Author manuscript; available in PMC 2018 May 15.

Published in final edited form as:

Dev Biol. 2017 May 15; 425(2): 208–222. doi:10.1016/j.ydbio.2017.03.032.

Brachyury drives formation of a distinct vascular branchpoint critical for fetal-placental arterial union in the mouse gastrula

Adriana M. Rodriguez[a], **Dexter X. Jin**[a], **Adam D. Wolfe**[b], **Maria M. Mikedis**[a], **Lauren Wierenga**[a], **Maleka P. Hashmi**[a], **Christoph Viebahn**[c], and **Karen M. Downs**[a,*]

[a]Department of Cell and Regenerative Biology, University of Wisconsin-Madison School of Medicine and Public Health, Madison, WI, USA

[b]Department of Pediatrics, Division of Pediatric Hematology, Oncology & Bone Marrow Transplant, University of Wisconsin-Madison School of Medicine and Public Health, Madison, WI, USA

[c]Institute of Anatomy and Embryology, University Medical Center Göttingen, Göttingen, Germany

Abstract

How the fetal-placental arterial connection is made and positioned relative to the embryonic body axis, thereby ensuring efficient and directed blood flow to and from the mother during gestation, is not known. Here we use a combination of genetics, timed pharmacological inhibition in living mouse embryos, and three-dimensional modeling to link two novel architectural features that, at present, have no status in embryological atlases. The allantoic core domain (ACD) is the extraembryonic extension of the primitive streak into the allantois, or preumbilical tissue; the vessel of confluence (VOC), situated adjacent to the ACD, is an extraembryonic vessel that marks the site of fetal-placental arterial union. We show that genesis of the fetal-placental connection involves the ACD and VOC in a series of steps, each one dependent upon the last. In the first, Brachyury (*T*) ensures adequate extension of the primitive streak into the allantois, which in turn designates the allantoic-yolk sac junction. Next, the streak-derived ACD organizes allantoic angioblasts to the axial junction; upon signaling from Fibroblast Growth Factor Receptor-1 (FGFR1), these endothelialize and branch, forming a sprouting VOC that unites the umbilical and omphalomesenteric arteries with the fetal dorsal aortae. Arterial union is followed by the appearance of the medial umbilical roots within the VOC, which in turn designate the correct axial placement of the lateral umbilical roots/common iliac arteries. In addition, we show that the ACD and VOC are conserved across Placentalia, including humans, underscoring their fundamental importance in mammalian biology. We conclude that *T* is required for correct axial positioning of the VOC via the primitive streak/ACD, while FGFR1, through its role in endothelialization and branching, further patterns it. Together, these genetic, molecular and structural elements safeguard the fetus against adverse outcomes that can result from vascular mispatterning of the fetal-placental arterial connection.

*Corresponding author. kdowns@wisc.edu (K.M. Downs).

Keywords

Allantoic core domain (ACD); Brachyury (T); Fibroblast Growth Factor Receptor 1 (FGFR1); Primitive streak; Vascular patterning; Vessel of confluence (VOC)

1. Introduction

In their transition to life on land, amniotes evolved a set of conserved extraembryonic tissues critical for survival in the shell or the maternal uterus. Among these, the allantois and yolk sac are required for successful exchange with the environment. In Placentalia, these vascular tissues form an integral part of the placentae. Their blood vessels arise independently in their respective sites (Arora and Papaioannou, 2012), and ultimately merge in the base of the allantois with those of the fetus, forming a circulatory continuum within the conceptus that ensures fetal survival during gestation. Despite its importance, the allantois-derived umbilical cord, which serves as the vascular conduit of nutrients, wastes and gases between the fetus and its mother, is one of the most understudied organs in placental mammals. Especially overlooked is how, within this vital structure, the umbilical and yolk sac blood vessels are connected to those of the fetus.

In the mouse, the allantois matures into the umbilical cord in a series of coordinated steps over a period of about 24 h (Inman and Downs, 2007). From the caudal end of the embryo, the allantoic bud forms, then extends, finger-like, toward the chorion. Its blood vessels are established *de novo* with distal-to-proximal directionality (Downs et al., 1998). Distally, the allantoic blood vessels form a diffuse network (Downs et al., 1998) that, as the allantois joins to and spreads across the chorion, rapidly penetrate the chorionic plate, transforming it from a flattened structure into a highly convoluted one to increase the surface area for exchange between the fetus and its mother. Proximally, the nascent umbilical vasculature is unbranched (Daane et al., 2011), a strategy that ensures union with the paired embryonic dorsal aortae and yolk sac omphalomesenteric artery at a single axial site, thereby promoting directed and efficient flow of blood into the umbilical cord to the chorionic disk.

While genetic control of the chorio-allantoic vascular connection at the distal end of the allantois has been fairly well documented (Inman and Downs, 2007; Watson and Cross, 2005), little is known about genetic, molecular and cellular regulation at the proximal end. Here, the allantois develops in intimate association with the fetus; consequently, abnormalities of the umbilical cord are often associated with defects in posterior fetal organs (Stevenson and Hall, 2006). While these observations highlight a developmental link in the etiology of socalled “orphan diseases”, not a single study has addressed how the fetal-placental connection is made.

Results of previous studies have, however, offered a few clues. Within the base of the allantois, at the site of its intersection with the yolk sac, morphological observations have suggested that arterial union may be mediated by a hitherto poorly documented hemogenic blood vessel, provisionally named the “vessel of confluence” (VOC) (Daane and Downs, 2011; Downs et al., 1998). Aside from its axial placement within the base of the allantois and hemogenicity (Daane and Downs, 2011), little more is known about the VOC.

The VOC appears during gastrulation (Downs et al., 1998). During this major morphogenetic period, the primary germ layers, ectoderm, mesoderm and endoderm, are deployed with respect to axial cues from the primitive streak and appropriately coalesce to form the nascent fetal organs. At its anterior embryonic end, the primitive streak condenses into Hensen's node, the ventral portion of which serves as a stem cell reservoir that creates the notochord, extending the embryonic body axis further anteriorly (Beddington, 1994). The node and notochord induce a variety of anterior structures, including the neural tube, somites and gut endoderm. However, the posterior end of the primitive streak, where the fetal-placental confluence is forged, had not, until recently, been satisfactorily identified in any species (Downs, 2009).

We had previously found that the mouse posterior primitive streak extends beyond the embryo proper and into the exocoelom (Downs et al., 2009; Inman and Downs, 2006a). As the allantoic bud forms, the extraembryonic streak expands into a Brachyury (T)-positive dense core, provisionally called the "allantoic core domain" (ACD) (Downs et al., 2009). Results of genetic, molecular and microsurgical approaches demonstrated that the ACD, like the node at the other end, emits an axial file of cells, and is required for allantoic extension to the chorion (Downs et al., 2009; Inman and Downs, 2006b). In addition, like the node, the ACD is a progenitor cell pool that, together with the embryonic component of the streak, supplies distinct tissues of the fetal-placental interface, including the VOC (Mikedis and Downs, 2012).

Intriguingly, and prior to our discovery of the ACD, we had reported that physical disruption of the allantoic T-domain along the anteroposterior axis, but not the dorsoventral one, severely compromised allantoic vasculogenesis (Inman and Downs, 2006b). These disruptions led us to believe that the base of the allantois contained anteroposterior signals that were involved in patterning the allantoic vasculature. We suggested that the presence of axial information within the allantois might be required to correctly position the umbilical vasculature with respect to that of the yolk sac and fetus (Downs, 2009). In that way, from the perspective of human health and disease, an organizational role of the primitive streak at the fetal-placental interface might explain and unify the etiology of a large number of birth defects that involve the umbilical vasculature and body axis in mouse models (Inman and Downs, 2007; Mikedis and Downs, 2014).

In this study, we hypothesized that the primitive streak/ACD is involved in organizing the fetal-placental vascular connection by correctly positioning the VOC along the axial midline. In turn, the VOC would form a fixed vascular site around which the fetal-placental confluence is established. To test this, we needed a means of creating defects in axial extension of the streak into the allantois, depriving it either of the full extent of the ACD or of the ACD itself, and then assaying the status of the VOC and subsequent fetal-placental arterial union. T was an attractive candidate for this investigation as *Tcurtailed* (T^C) mutants were shown to exhibit dose-dependent reduction/extension of the anteroposterior axis, as assayed by tail length in neonates (Stott et al., 1992). Dose-dependency can result either from loss of function, as in the classical T deletion (Herrmann et al., 1990), or from dominant-negative interference due to mutations within the allele, as in the case of T^C (Stott et al., 1992). In either case, what is important is how much gene product or protein is

available for function. Given that we did not carry out biochemical analysis of that availability, we have adopted the term “dose-dependency” as used by Stott and colleagues to refer to the correlation between phenotype and the number of normal copies of *T*. In addition, as creation of an organized vascular network requires FGFR1 signaling (Lee et al., 2000; Magnusson et al., 2004), we assayed for the presence of FGFR1 in the prospective VOC, and then devised a pharmacological method to assess FGFR1 function in patterning the fetal-placental confluence in living embryos. Finally, the posterior region of several placental mammals, including the rabbit, pig and human, was examined for evidence of conservation of an ACD-like dense core and VOC across Placentalia.

2. Materials and methods

2.1. Animals and husbandry

Animals were treated in accordance with Public Law 99–158 as enforced by the University of Wisconsin-Madison or in accord with the German Animal Protection Law. Timed matings (Downs, 2006) produced staged mouse embryos. Inbred hybrid F2 conceptuses (parental B6CBAF1/J, Jackson Laboratory, Bar Harbor, ME) were used for most experiments. *Flk-1:lacZ* heterozygous conceptuses were maintained as previously described (Downs, 2008). Conceptuses resulting from intercrossing T^{C}/T^{+} animals were biopsied and genotyped as previously described (Inman and Downs, 2006b). Rabbits (*Oryctolagus cuniculus*; New Zealand White strain) were obtained from Charles-River (Geislingen, Germany) (Blum et al., 2007) and pigs (*Sus scrofa domesticus*) from the Faculty of Agricultural Sciences (Gottingen, Germany) (Hassoun et al., 2009).

2.2. Dissection, staging, and whole mouse embryo culture

Embryo dissection, staging (upper right, figure panels), and whole embryo culture (initial/final stage, upper right, figure panels) were as previously described (Downs, 2006; Downs and Davies, 1993). Mouse stages examined were: late streak (LS; ~E6.75-7.0), neural plate/no allantoic bud (OB; ~E7.0), neural plate/early allantoic bud (EB; ~E7.25), neural plate/late allantoic bud (LB; ~E7.5), early headfold (EHF; ~E7.75), late headfold (LHF; ~E8.0), and 1–11 somite pairs (s; ~E8.25-E9.0). Dissection and staging of rabbits and pigs were as described (Blum et al., 2007; Hassoun et al., 2009). Human conceptuses were not dissected, but downloaded from the Digitally Reproduced Embryonic Morphology (DREM) database (http://virtualhumanembryo.lsuhsc.edu/DREM/OnlineDisks.html). Human stages (O’Rahilly and Müller, 2010) and embryo numbers were: CS6 (primitive streak stage, ~16–18 days): No. 7801; CS7 (neural plate stage, ~18–21 days): No. 7802; CS8 (neural fold stage, ~21–25 days): No. 10157.

2.3. Attenuation of FGFR1 signaling

Two pharmacological inhibitors, placed into the medium just prior to culture, attenuated FGFR1 signaling.

***PD173074* (Sigma, St. Louis, MO; P2499)—**A 40 mM stock solution in DMSO (dimethyl sulfoxide; Sigma, D5879) was stored at 4 °C. Just prior to use, the stock solution was diluted 1:1000 in dissection medium (Downs, 2006), after which 1 μl of this working

solution was further diluted in 1 ml culture medium (Downs, 2006) for a final concentration of 40 nM PD173074. This final concentration of DMSO was not toxic in vehicle controls (data not shown).

***Chlorate* (Sigma, 410241)—**A 2 M stock solution in tissue culturegrade water was stored in aliquots at −20 °C. After thawing, 5 μl was added to 1 ml culture medium for a final concentration of 10 mM chlorate. Untreated and vehicle controls displayed no defects after culture (data not shown).

Application: Conceptuses were exposed in culture to PD173074 or chlorate before or after formation of the VOC at twelve morphological stages (late-streak, no allantoic bud, early/late bud, early/late headfold, 1–6-somite pairs), which were separated by 2–4 h. Prior to deciding upon a final concentration of each inhibitor, above, several concentrations were assessed (data not shown). While 1 μM PD173074 recapitulates defects in early gastrula-stage *Fgfr1*$^{-/-}$ mutants (Oki et al., 2010), we found that conceptuses exposed to this high concentration exhibited severe structural loss of tissue at the posterior embryonicextraembryonic interface, thereby precluding assessment of vascular defects there. Also, PD173074's specificity for FGFR1 is concentrationdependent (Mohammadi et al., 1998); at 1 μM, PD173074 abrogates not only FGFR1 signaling, but also that of Vascular Endothelial Growth Factor (VEGF) (Mohammadi et al., 1998). By contrast, we found that 40 nM PD173074, which is in the reported range of specificity for attenuating FGFR1 (Mohammadi et al., 1998), optimally eliminated pFGFR1 in the prospective VOC while maintaining adequate posterior development throughout the culture period. Application of 40 nM PD173074 at the bud stages, prior to VOC formation, led to failure of vascular continuity within the posterior embryonic-extraembryonic interface, providing early insight into the timing of VOC initiation and role in forging the fetal-placental connection. Similar to 40 nM PD173074, 10 mM sodium chlorate preserved embryonic development, while application of high concentrations (20–50 mM) prior to VOC formation resulted in grossly stunted embryos, which died at the end of culture.

Affect on T—*Fgfr1*$^{-/-}$ conceptuses were claimed to display generalized expansion of the *T* domain (Deng et al., 1994; Yamaguchi et al., 1994), which was "down-regulated" in the primitive streak of *Fgfr1*$^{-/-}$ mutants (Ciruna and Rossant, 2001). In the latter, these specimens would be expected, in whole mount preparations, to appear negative for T. However, we found by histology that conceptuses treated with 1 μM PD173074 were devoid of the embryonic component of the streak (data not shown). By contrast, 40 nM PD173074 did not affect T localization within the streak or within the ACD, both of which, by morphology, were present and exhibited T (data not shown). The only aberrancy noted was that, at later somite stages, T persisted in the ACD when it should have been attenuated or cleared (Downs et al., 2009) (data not shown).

2.4. X-gal staining and immunohistochemistry (IHC)

A standard protocol (Downs, 2006) identified *lacZ* expression in *flk-1: lacZ* reporter conceptuses. IHC was as previously described (Downs, 2008). Primary antibodies, sources, stock concentrations, dilutions, and Research Resource Identifiers (RRIDs) were: **Bi-**

Phospho-FGFR Y653/654 (pFGFR1) (AP3104A, Abgent, San Diego, CA; 0.25 mg/ml, rabbit polyclonal; 1/60 dilution; RRID: AB_ 636986); **BRACHYURY (T)** (sc-17743, Santa Cruz Biotechnologies, Santa Cruz, California; 200 μg/ml, goat polyclonal; 1/100 dilution; RRID: AB_634980); **CASPASE-3 (CASP3)** (559565, BD Biosciences, San Jose, California; 0.5 mg/ml, rabbit monoclonal; 1/100 dilution; RRID: AB_397274); FGF2 (sc-79-G, Santa Cruz Biotechnologies; 200 μg/ml, goat polyclonal; 1/50 dilution; RRID: AB_631498); **FGFR1** (ab10646, Abcam, Cambridge, MA; 1500 μg/ml, rabbit polyclonal; 1/400 dilution; RRID: AB_297367); **FGFR2** (sc-122-G, Santa Cruz Biotechnologies; 200 μg/ml, goat polyclonal; 1/300 dilution; RRID: AB_631510); **FGFR3** (sc-123-G, Santa Cruz Biotechnologies; 200 μg/ml, goat polyclonal; 1/300 dilution); **FLK-1** (sc-315-G, Santa Cruz Biotechnologies; 200 μg/ml, goat polyclonal; 1/50 dilution; RRID: AB_632599) (Inman and Downs, 2006b); **OCT-3/4** (sc-8628, Santa Cruz Biotechnologies; 200 μg/ml, goat polyclonal; 1/100 dilution; RRID: AB_653551); and **PECAM-1** (AF3628, R & D Systems, Minneapolis, MN; 0.2 mg/ml, goat polyclonal; 1/500 dilution; RRID: AB_2161028). Secondary antibodies were: donkey anti-rabbit (sc-2089, Santa Cruz Biotechnologies; 0.4 mg/ml; 1/500 dilution; RRID: AB_641178) and donkey anti-goat (sc-2042, Santa Cruz Biotechnologies; 0.4 mg/ml; 1/500 dilution; RRID: AB_631726). The BRACHYURY antibody did not distinguish between wildtype and *Curtailed* alleles (Inman and Downs, 2006b). Specificity of the FGFR1 (ab10646), FGFR2 (sc-122) and FGFR3 (sc-123) antibodies was verified with comparisons of staged-matched specimens (FGFR1, 2: EHF stage; FGFR3: 4s stage) that were subjected in parallel to IHC in four treatment groups, as previously described (e.g., Downs et al., 2009): (i) standard application of the antibody, just prior to the overnight rocking step (FGFR1: n=3; FGFR2, 3: n=1); (ii) 8-h incubation of the primary antibody alone at 4 °C (FGFR1: n=3; FGFR2, 3: n=1) prior to application to the specimens; (iii) 8-h incubation of the primary antibody with 10–15 times more cognate peptide (FGFR1: ab71927, n=3; FGFR2: sc-122P, n=2; FGFR3: sc- 123P, n=2) than primary antibody at 4 °C prior to application to the specimens; and (iv) absence of the primary antibody (FGFR1: n=3; FGFR2, 3: n=1). Immunostaining was comparable in the standard and 8 h incubation groups; by contrast, no immunostaining was observed in the cognate peptide + antibody and minus antibody groups, thereby confirming specificity of the antibodies used.

2.5. Immunofluorescence (IF) and fluorescent imaging

IF was as previously described (Mikedis and Downs, 2013). Primary antibody sources, stock concentrations, dilutions, and RRIDs were: BRACHYURY (T) (1/25 dilution), Bi-Phospho-FGFR Y653/654 (pFGFR1) (SAB1306302, Sigma; 0.42 mg/ml, rabbit polyclonal; 1/10 dilution). Secondary antibodies were: Dylight 550-conjugated donkey anti-goat (ab96932, Abcam; 0.5 mg/ml; 1/100 dilution; RRID: AB_ 10680411); Dylight 650-conjugated donkey anti-rabbit (ab98501, Abcam; 0.5 mg/ml; 1/100 dilution; RRID: AB_10676120). After incubation with DAPI (D1306, Life Technologies, Fitchburg, WI; stock 5 mg/ml; 1/830 dilution; RRID: AB_2629482) and subsequent washes, samples were stored at 4 °C and mounted (Mikedis and Downs, 2013) within 3 days. Fluorescent images were collected with a Nikon A1R+ confocal microscope (W.M. Keck Laboratory for Biological Imaging, UW-Madison) using a CFI Plan Apo Lambda 60x oil objective, a pinhole size of 1.2 AU, and lasers at 408, 561, and 638 nm.

2.6. Histological analysis of mouse, rabbit, pig and human

Mouse conceptuses were prepared for histology as previously described (Daane et al., 2011). Histological sections of rabbit and pig conceptuses were analyzed and imaged from a collection of 1 μm thick plastic sections (University of Göttingen), which were processed as previously described (Blum et al., 2007; Hassoun et al., 2009). Analysis included examination of 8 rabbit conceptuses (stages: 3–25s, ~E7.7- E9.0) and 14 pig conceptuses (stages: 2–15s, ~E13.0-E15.0). Analysis of human conceptuses was carried out on transverse histological sections downloaded from the DREM database. The 3D volume rendered surface models displayed in insets of Fig. 6**I, J** were obtained from the DREM database.

2.7. Three-dimensional (3D) modeling

3D reconstruction of histological sections was carried out using the Amira software system (Visualization Sciences Group, Burlington, MA). Sequential images were loaded into Amira and made into an object with 3D pixel (voxel) dimensions of 1×1×6 voxels (1 μm=1 voxel). Slices were then re-aligned in pair-wise fashion and resampled. Structures of interest were labeled with tissue-specific colors one slice at a time (Fig. 2**H–K**). After labeling all slices, the surface generator computed a free-form surface model from which snapshots for the 3D models were taken. Reconstruction of the fetal-placental interface in mouse conceptuses began at the closed hindgut, with serial transverse sections added posteriorly toward the umbilical artery (including 5 sections of the proximal umbilical artery; Fig. 2**L–N** and Fig. 5**A–D, O–R**) or the end of the embryonic tail (Fig. 3**A, C, E**); for younger specimens (Fig. 2**E, F**), which had yet to form a hindgut, reconstruction encompassed 33 sections spanning the posterior embryonicextraembryonic interface. Boundary limits for the VOC were set in these serial transverse collections. For specimens ≤6s (Fig. 2**E, F**), the VOC was located just dorsal to the allantoic-yolk sac junction. For specimens ≥7s (Fig. 2**L–N** and Fig. 5**A–D, O–R**), the VOC was defined by its branching pattern, either dorsally to the dorsal aortae or ventrally to either the umbilical or omphalomesenteric arteries.

2.8. Measurements

For all measurements, the amnion was designated as the topographical equator between the embryonic and extraembryonic components of the posterior region (Lawson et al., 1991). Length measurements were acquired with the length tool on the NIS Elements software. Placement of the allantoic-yolk sac junction was measured as the vertical distance from the amnion to the allantois' insertion into the yolk sac mesoderm (positive length, extraembryonic territory; negative length, embryonic territory). The length of the ACD was taken as the vertical distance from the allantoic site of insertion into the amnion to the distalmost end of the allantois' T-positive core. The length of the umbilical artery was taken from its site of exposed insertion into the fetus to its distal insertion into the chorion, while the length of the lateral umbilical roots was taken from their site of insertion into the fetus to their branchpoint on the umbilical artery.

Hindgut size was evaluated based on its volume, which was calculated from measuring the area of the hindgut in each transverse section it spanned with the area tool on the NIS Elements software (Nikon, Tokyo, Japan), multiplying these sectional areas by their sectional thickness (6 μm) and summing these values for a total hindgut volume.

2.9. Statistical analysis

For all experiments, n ≥3 for all stages and all genotypes. Analysis for differences between group means was carried out via two-tailed Student *t*-Tests with significance at $P < 0.05$.

3. Results

3.1. The posterior limit of the primitive streak, allantoic-yolk sac junction, and site of VOC formation intersect during the bud stages

Fig. 1**A** codifies previous observations with the goal here of providing a framework for understanding the mechanism of formation of the fetal-placental confluence. At the pre-bud stages, the primitive streak extends into the exocoelom, and is closely applied to the visceral endoderm, called allantois-associated visceral endoderm (AX) (Downs et al., 2009). As the allantoic bud forms, the streak maintains full contact with the AX; its posterior limit coincides with the allantois' ventral connection to the yolk sac mesoderm. We have designated this posterior site as the "allantoic-yolk sac junction". By the headfold stages, when the streak expands into the allantoic core domain (ACD), the allantois separates from the yolk sac, creating a new, more anteriorly (i.e., proximally) placed allantoic-yolk sac junction and becoming shaped into a distinct finger-like projection through which the ACD partially extends within the allantoic midline. Over the next few hours, even though the allantois lengthens, the ACD itself remains stable, maintaining its original size (Downs et al., 2009). As allantoic elongation continues (2–3s), the allantoic-yolk sac junction is gradually re-positioned toward the embryo, concomitant with apparent progressive reduction in the length of the AX, which seems ultimately to be incorporated into the hindgut portal by 4s (Downs, 2008; Downs et al., 2009). At this time, the vessel of confluence (VOC) was noted in all specimens examined, and was situated at the allantoic-yolk sac junction (Downs et al., 1998).

In our first set of experiments, we sought to refine this working blueprint by identifying the earliest time at which prospective VOC angioblasts were present at the axial midline. During the pre- and bud stages, the posteriormost limit of the streak, the allantoic-yolk sac junction, and a cluster of prospective VOC T-positive angioblasts, were all found at the same site (Fig. 1**B**). As the ACD formed at the headfold stages, the allantois separated from the yolk sac, creating a new allantoic-yolk sac junction (Fig. 1**C**). The prospective VOC remained fixed at the junction, but was now ventral to the primitive streak/ACD, rather than located at its distal tip (Fig. 1**B, C**); it was composed of a mixture of T-positive and T-negative angioblasts. Between 2s and 4s, an endothelialized VOC, which was negative for T, was invariably present within the axial midline just beneath the allantoic-yolk sac junction (Fig. 1**D, E**).

3.2. Brachyury (T) positions the allantoic-yolk sac junction and the VOC

As the allantoic-yolk sac junction coincided with the posterior limit of the primitive streak at the pre- and allantoic bud stages, we asked whether the primitive streak positions this junction, and thus, the VOC. For this, we examined the junction and VOC in *T-curtailed* (T^C) littermates.

Taking the amnion as the horizontal divide between the embryonic and extraembryonic regions (see Section 2.8), we compared the initial length of the primitive streak in the three T^C genotypes, wildtype, heterozygotes, and homozygotes, after it had extended into the exocoelom (pre- and bud stages) (Fig. 1**F–I**). In all three genotypes, the position of the allantoic-yolk sac junction correlated with the extent to which the streak had reached into this cavity. T^+/T^+ wildtype specimens, with two normal copies of *T*, exhibited the most posterior placement of the streak, and thus, the posteriormost placement of the allantoic-yolk sac junction with respect to the embryo (Fig. 1**F, I**). By contrast, T^C/T^C homozygotes, with no normal copies of *T*, exhibited the most truncated streak, which hardly reached into the exocoelom, resulting in extreme anterior positioning of the allantoic-yolk sac junction toward the embryo (Fig. 1**H, I**). As the streak's extension fell between these two extremes in T^C/T^+ heterozygotes, which bear one normal copy of *T*, placement of allantoic-yolk sac junction was intermediate between that of T^+/T^+ wildtype and T^C/T^C homozygotes (Fig. 1**G, I**).

Next, the streak-derived ACD was examined (Fig. 1**J–M**). In T^+/T^+ wildtype specimens, the ACD was fully expanded within the allantois and associated with a ventrally positioned VOC, which remained within the extraembryonic region (Fig. 1**J, K**). In T^C/T^+ heterozygotes, the ACD was shortened, though an axially located VOC was still present ventral to it. However, the allantoic-yolk sac junction was aberrantly located within embryonic territory, as determined by its relationship to the amnion (Fig. 1**J, L**). In T^C/T^C homozygous mutants, the ACD was absent within what remained of the allantois, and the allantoic-yolk sac junction was even more extremely positioned anteriorly within the embryo proper. Moreover, an axially located VOC was undetectable at the midline (Fig. 1**J, M**). It is worth pointing out that previous studies showed that the anterior notochord was present in *T/T* deletion mutants, though fragmenting (Chesley, 1935). Here, we confirmed via T immunostaining, the antibody of which recognizes the T^C protein (see Section 2.4) that the anterior notochord was present, though fragmenting, in T^C/T^C homozygotes through 6–9s (data not shown); moreover, similar to *T/T* (Herrmann, 1991), T^C was not detectable in the posterior primitive streak and developing posterior node, though we did not confirm the presence/absence of these structures by any other means (data not shown).

Given these observations, we followed the allantoic-yolk sac junction over time. As development progressed from pre- and bud stages through early somites, placement of the junction shifted anteriorly toward the embryo in all genotypes with respect to the amniotic embryonic-extraembryonic junction (Fig. 1**I, N**). While this shift appeared to be a normal morphogenetic consequence of allantoic elongation and simultaneous development of the underlying hindgut pocket, the junction remained within the extraembryonic region of wildtype conceptuses, but came to lie aberrantly within the embryonic compartment of T^C/T^+ heterozygous and T^C/T^C homozygous mutants (Fig. 1**I, N**), with anterior placement most severe in the homozygotes.

Cell death was not likely the cause of apparent loss of the VOC in the T^C/T^C homozygotes (Fig. 1**M**), as there were no differences in the number of CASP-3-positive cells amongst the three genotypes at all stages examined (Fig. 2**A**). Inspection of serial histological sections revealed that angioblasts were appropriately localized to the distal allantois and prospective

VOC in wildtype and heterozygous specimens (n=3 per genotype, early headfold stage) (Fig. 2**B, C**). However, one of three T^C/T^C mutant specimens examined at a similar stage displayed a laterally misplaced endothelialized vessel within the yolk sac itself at the allantoic-yolk sac junction (Fig. 2**D**). Given that yolk sac vessels, prior to somitogenesis, are limited to the blood ring (McGrath et al., 2003) which lies near the chorion, this small vessel was likely a misplaced VOC. This possibility was borne out at 4s, when 3D reconstruction of serial sections revealed that all T^C/T^C mutants (n=4/4) presented a laterally positioned vessel at the allantoic-yolk sac junction with no left-right bias (Fig. 2**E–G**).

3D reconstructions of the vasculature at the fetal-placental interface at later stages (Fig. 2**H–K**) showed that the normal VOC bifurcates at its dorsal end to join the left and right branches of the paired dorsal aortae, while at its ventral end, the VOC branches posteriorly (i.e., distally) to join the umbilical artery, and anteriorly (i.e., proximally) to unite with the omphalomesenteric artery (Fig. 2**L**). Only T^+/T^+ wildtype and T^C/T^+ heterozygous littermates exhibited the mature fetal-placental vascular confluence, referred to hereafter as the “OUA connection” (O, omphalomesenteric artery; U, umbilical artery; A, aorta) (Fig. 2**L, M**). An axial OUA connection was missing in T^C/T^C mutants, which also displayed an umbilical artery that, while endothelialized, was fragmented and aberrantly positioned off the midline (Fig. 2**N**).

Together, these results show that loss of an axially placed VOC leads to loss of the OUA connection. Two normal copies of *T* were required to position the allantoic-yolk sac junction to the correct axial level; in this way, the VOC was maintained within the extraembryonic territory. One normal copy of *T* was sufficient to ensure adequate expansion of the ACD in the allantois so as to axially organize allantoic angioblasts to the allantoic-yolk sac junction. However, in the heterozygotes, the axial VOC was abnormally positioned within embryonic territory. Without any normal copies of *T*, the allantoic-yolk sac junction was even more anteriorly positioned in the embryo. In addition, the ACD was absent, and allantoic angioblasts were not organized into an axially-placed VOC.

3.3. The medial umbilical roots may arise from the VOC during remodeling and designate the site of axial sprouting of the aorta-derived lateral umbilical roots

In normal development, the first major vascular remodeling process of the OUA connection occurs between E8.75 (~10s) and E9.25 (~15s), as the embryo turns to acquire the traditional fetal position (Walls et al., 2008). As the tailbud increases in size, the base of the allantois shifts anteriorly, bringing the fixed vascular confluence with it. This causes the dorsal bifurcation of the VOC to extend ventrally, the branches of which then curve around the expanding hindgut (Fig. 3**A, B**). As the origin of these curving branches is obscure, previous reports have referred to them as the “re-curved portions of the dorsal aortae” (Garrido-Allepuz et al., 2012; Zakin et al., 2005) or the “medial umbilical roots” (Gest and Carron, 2003).

Analysis of T^C littermates during the embryonic turning period (Fig. 3**A–G**) revealed that the medial umbilical roots were present in T^+/T^+ wildtype and T^C/T^+ heterozygous embryos (Fig. 3**A–D**), but foreshortened in the latter (Fig. 3**C, D**). Nevertheless, an OUA connection

formed in both. Foreshortening of the medial umbilical roots was not due to a reduction in the hindgut, as only T^C/T^C mutants exhibited hindgut reduction (Fig. 3**G**). Rather, foreshortening was consistent with earlier anterior misplacement of the VOC within the embryonic territory. By contrast, the medial umbilical roots were altogether absent at the midline in T^C/T^C mutants, likely due to axial misplacement of the VOC at earlier stages (Fig. 3**E, F**). Consequently, an organized axial OUA connection was missing. In its place, the dorsal aortae and omphalomesenteric artery, which were not affected by loss of *T*, fused with the fragmented umbilical artery to create a severely abnormal confluence.

T^C/T^C embryos die between E9.5-E10.5 (Inman and Downs, 2006b) and could not be studied further. T^C/T^+ heterozygotes, however, survive through birth, but exhibit posterior defects that are compatible with life (Searle, 1966). Thus, T^C/T^+ heterozygotes were examined during the next major vascular remodeling event. In normal development, the medial umbilical roots regress between E10.0 and E13.5 to become the caudal mesenteric artery in the mouse (Gest and Carron, 2003), or the inferior mesenteric artery in humans (Gest and Carron, 2003). At the same time, the aorta sprouts the lateral umbilical roots, which are positioned with respect to the regressing medial ones, where they take over the connection between the aorta and umbilical artery (Gest and Carron, 2003). These lateral umbilical roots ultimately become the common iliac arteries (Gest and Carron, 2003) that divide the flow of blood from the aorta into each hindlimb. Comparison of T^+/T^+ and T^C/T^+ specimens showed that, while the length of the umbilical artery was the same in all littermates (Fig. 3**H**), the heterozygotes exhibited shortened lateral umbilical roots (Fig. 3**H–J**). Foreshortening was likely due to a downstream domino effect that began with anterior misplacement of the VOC.

3.4. Activated FGFR1 uniquely localizes to the prospective VOC

Up to this point, we have shown that *T* is required for extension of the primitive streak, which in turn creates the allantoic-yolk sac junction, thereby positioning the prospective VOC to this site. The ACD maintains the VOC in an axial position at the allantoic-yolk sac junction. We have assumed that the VOC is a unique blood vessel, formed independently of the major arterial vessels that it brings together. However, we have not formally demonstrated this.

The Fibroblast Growth Factor family plays a variety of roles in the biology of mesoderm (Dorey and Amaya, 2010). Intriguingly, of three FGF receptors, FGFR1, FGFR2, and FGFR3, only FGFR1 robustly localized to the prospective VOC (OB-2s stages) (Fig. 4**A–C**). At the headfold stages, both FGFR1 and FGF2, the ligand known to stimulate FGFR1's vascular function (Cox and Poole, 2000; Lee et al., 2000; Magnusson et al., 2004), were found in prospective VOC angioblasts (Fig. 4**C, D**), arranged as rosettes (Fig. 4**C**). This profile was tantalizing, as rosette structures are the precursors of *de novo* branching points during tumor angiogenesis and represent a key feature in the formation of new blood vessels (Seano et al., 2014). By 4–6s, when the VOC had endothelialized, FGFR1 was no longer detectable in this region (data not shown).

Activated phosphorylated FGFR1 (pFGFR1) localized to *flk-1*-positive angioblasts of the prospective VOC just as the allantoic bud was beginning to form (Fig. 4**E**); FLK-1 is a major

receptor for vascular endothelial growth factor (VEGF), and is found in most, if not all, angioblasts (Dumont et al., 1995). As the allantois elongated, pFGFR1- positive angioblasts coalesced and flattened, forming the mature VOC (Fig. 4**F**). Like T, pFGFR1 was undetectable in the VOC after its endothelialization (Fig. 4**G**). pFGFR1 and T co-localized within some, but not all, VOC angioblasts (Fig. 4**H–K**), suggesting the possibility of co-dependency in VOC formation.

3.5. The VOC is a unique vessel whose endothelialization and branching require FGFR1

With a systematic spatiotemporal cellular and molecular blueprint in hand, we sought to abrogate FGFR1 signaling to discover its role in VOC formation and/or patterning. Unfortunately, *Fgfr1*$^{-/-}$ conceptuses die as early as E7.5 due to defective mesodermal patterning (Böttcher and Niehrs, 2005; Deng et al., 1994; Yamaguchi et al., 1994) and thus, do not survive long enough to allow study of VOC genesis. Therefore, use of *Fgfr1*$^{-/-}$ conceptuses for this study was out of the question. To circumvent this, we exploited our morphological and molecular timecourse of VOC formation (Fig. 1**B–E** and Fig. 4**E–G**) so as to time the application of pharmacological inhibitors and discover the role of FGFR1 in VOC formation.

PD173074 inhibition (see Section 2.3) began at the pre-bud stages (late streak and neural plate/no allantoic bud; see Section 2.2), as the primitive streak is reaching into the exocoelom. Thereafter, PD173074 was applied at each successive developmental stage, all of which were separated by 2–4 h, until 6s, which is several hours after formation of the VOC. Treated conceptuses were cultured alongside untreated controls until the 7–8s stages, at which time the VOC should have been engaged in arterial union with the surrounding vessels.

3D reconstructions (Fig. 5**A–D**) of the posterior vasculature consistently revealed three profiles, dependent upon the timing of FGFR1 inhibition (Fig. 5**E**): complete loss of the vascular confluence (Fig. 5**B**), incomplete vascular confluences (Fig. 5**C**), and normal confluences (Fig. 5**D**). Complete loss of the vascular confluence was invariably observed when PD173074 was applied at the pre-bud stages (Fig. 5**A, B, E**). While the major arterial vessels were present at the end of culture, they failed to unite, as the VOC appeared to be missing (Fig. 5**B**). Applications of PD173074 at the slightly later bud stages resulted in a mixture of these profiles (Fig. 5**B, E**). Among the incomplete confluences, either the umbilical artery or the dorsal aortae failed to connect via the VOC. This suggested that, in these cases, the VOC had failed to properly branch and meet these vessels to unite them. The umbilical artery (Fig. 5**E** and data not shown) or the dorsal aortae (Fig. 5**C, E**) were often joined to the omphalomesenteric artery via an incompletely branched VOC. By early somite stages, all treated specimens exhibited normal and complete confluences (Fig. 5**A, D, E**).

To fully appreciate the role of FGFR1 in genesis of the VOC, prebud stage specimens were again exposed to PD173074, only this time, they were cultured for short timeperiods, after which embryos were examined for the status of a nascent endothelialized VOC. In inhibited specimens, angioblasts were present at the allantoic-yolk sac junction, but they had not coalesced or flattened to form a mature vessel, even though they were at the correct stage to

have done so (Fig. 5**F, G**). Failure of angioblasts to endothelialize was not the result of misregulation of *T* because, as in the controls, prospective VOC angioblasts appropriately cleared *T*'s cognate protein and therefore, must have been on their way toward endothelialization (Fig. 5**H, I**). Moreover, T^C mutants exhibited no change in pFGFR1 at the allantoic-yolk sac junction (Fig. 5**J–L**). In addition, the stem cell potency regulator, OCT-3/4 (Niwa et al., 2000), which also co-localizes with fl*k-1* in the allantois (Downs, 2008), has a profile similar to that of T, being found in VOC angioblasts but diminishing as they mature (Downs, 2008). Here, in the presence of the PD173074 inhibitor, OCT-3/4, like T, was also appropriately cleared in the prospective VOC (Fig. 5**M, N**), indicating that loss of the VOC was not due to failure of VOC angioblasts to mature and differentiate.

Cultures using chlorate as an inhibitor of extracellular matrix heparan sulfate synthesis (Lin, 2004) supported the results of PD173074 inhibition. Chlorate-treated conceptuses exhibited complete and specific loss of the OUA connection during applications at early stages (Fig. 5**O, P, S**), due also to failure of VOC angioblasts, which were present, to endothelialize (Fig. 5**T–V**). However, consistent with chlorate's lack of specificity (Lin, 2004), complete loss of the VOC was initially limited to ~20% of pre-bud specimens (Fig. 5**S**). About 30% exhibited incomplete VOC-driven confluences (Fig. 5**Q, S**) while the rest were normal (Fig. 5**R, S**). At the 2s stage or later, all chlorate-treated specimens were normal (Fig. 5**R, S**), similar to PD173074 treatment.

Finally, we asked whether attenuation of pFGFR1 resulted in axial misplacement of the allantoic-yolk sac junction, as observed in T^C/T^C and T^C/T^+ mutants. Application of PD173074 at the pre-bud stages, followed by short-term culture and analysis (headfold-1s stages), revealed no significant differences (P=0.671; Student *t*-Test) in placement of the junction between treated (n=13) and control specimens (n=6).

Collectively, these results reveal a number of valuable conclusions regarding how the VOC, under the regulation of pFGFR1 signaling, drives genesis of a correctly patterned fetal-placental arterial union. First, the VOC is a singular vessel that forms via pFGFR1 signaling during a well-proscribed but very narrow period of gastrulation. Complete loss of the VOC upon PD173074 application at pre-bud stages, followed by gradual restoration of a fully-mature VOC when applied at later stages is consistent with our finding that the VOC forms over time. Second pFGFR1 is required for endothelialization and branching of the VOC, enabling it to meet the major arterial vessels to unite them. Third, pFGFR1 is not required either for the formation of the arterial vessels to which the VOC joins or for correct axial placement of the VOC. Lastly, given the presence of pFGFR1 within the angioblasts of the prospective VOC in all three T^C genotypes as well as the normal profile of T in pFGFR1-inhibited VOC angioblasts, FGFR1 and T likely carry out independent functions there.

3.6. The VOC is conserved in placental mammals and is invariably associated with a dense allantoic core

In light of our results demonstrating the critical importance of the VOC in organizing the mouse fetal-placental confluence, we asked whether this unique vessel was conserved in other placental mammals and whether conservation was associated with an allantoic dense core. Toward this end, we examined histological sections of the posterior region of the

rabbit, pig and human, comparing them with genesis of the mouse VOC and OUA (Fig. 6**A-C**).

In the rabbit (Fig. 6**D, E**), pig (Fig. 6**F–H**), and human (Fig. 6**I–K**), a similar axially positioned small vessel was found adjacent to a dense allantoic core (Fig. 6**D, F, G, I**). As in the mouse (Fig. 6**A**), the dense core in the rabbit (Fig. 6**D**) and pig (Fig. 6**F, G**) was contiguous with embryonic mesoderm, while in the human conceptus, it was part of the axial endodermal core/allantoic diverticulum (Fig. 6**I**). Given its dense morphology and topographical position, the dense core in these nonrodent animal models may possibly represent the extraembryonic component of the primitive streak, or mouse ACD.

At later stages in the mouse, rabbit and pig, the OUA connection was composed of the full panoply of posterior arterial vessels (Fig. 6**B, C, E, H**) and still associated with a dense allantoic core; by contrast, in the one human specimen available, only the nascent umbilical and omphalomesenteric arteries were initially joined at the VOC (Fig. 6**J**), and associated with morphologically transitional visceral endoderm of the yolk sac (Fig. 6**K**), which defines the embryonic-extraembryonic junction in the mouse (Fig. 6**A**) (Bonnevie, 1950). This partial confluence provided early clues into the sequence by which the posterior arterial vessels might join, especially as a previous report confirmed that, at the next stage, the dorsal aortae were united with the placental arterial blood vessels (Ingalls, 1920).

From these observations, we conclude that, in all placental mammals thus far examined, a dense allantoic core and VOC are conserved across species and associated with the posterior end of the primitive streak at the allantoic-yolk sac junction where the mature OUA connection is later established.

4. Discussion

4.1. Genesis of the fetal-placental confluence is dependent upon T's ability to ensure adequate extension of the body axis into the extraembryonic region and on FGFR1's role in VOC endothelialization and branching

Genesis of the mature fetal-placental confluence is summarized in Fig. 7. In the first step, two normal copies of *T* are required for full extension of the streak into the exocoelom, establishing there the position of the allantoic-yolk sac junction. As the allantoic bud forms, T-positive/pFGFR1-positive angioblasts cluster at this axial junction (Fig. 7**A**). By the headfold stages (Fig. 7**B**), the primitive streak expands into the ACD (Downs et al., 2009). If the streak has not fully extended, as in T^{+}/T^{C} heterozygotes, a partial ACD nevertheless forms, and is sufficient to organize allantoic angioblasts at the midline, albeit to a more anterior (proximal) position. Loss of two normal copies of *T*, as in T^{C}/T^{C} homozygous mutants, leads to loss of the ACD and failure of allantoic angioblasts to become organized into an axially-placed VOC and umbilical artery. Thus, *T* is not required for angioblast formation or endothelialization, but it is required for axial positioning of major allantoic vascular components, the VOC and umbilical artery. Previous studies of the *T-curtailed* mutant showed that tail length was dosedependent on the number of copies of normal *T* present (Stott et al., 1992). These authors assumed that axial elongation was involved but had not shown defects in the streak. Here we have formally demonstrated that *T* is required

for extension of the primitive streak into the extraembryonic region where it organizes the VOC and umbilical artery.

Over time, only a subset of prospective VOC angioblasts exhibited T (Fig. 7**B**); whether this population is heterogeneous is not known, but at least some VOC component cells arise from the ACD (Mikedis and Downs, 2012) and may be in dynamic flux, appearing non-uniform at any given time. Whatever the case, prospective VOC angioblasts downregulate both T and pFGFR1, and by 2–4s, endothelialize into the mature VOC (Fig. 7**C**). Given that T and pFGFR1 co-localized in some prospective VOC angioblasts, we asked whether these two proteins worked together in building the VOC, and/or formed a molecular hierarchy. The status of pFGFR1 was examined in T^{C} mutant scenarios while conversely, T was examined in FGFR1-inhibited scenarios. In both cases, we found no evidence that T or pFGFR1 were compromised. Thus, we conclude that T and FGFR1 do not operate together or in hierarchical manner in prospective VOC angioblasts, but rather independently of the other.

Endothelialization and branching (Fig. 7**D**), both of which required pFGFR1, resulted in the VOC's reaching out to the major arterial blood vessels and uniting them. The umbilical, omphalomesenteric and fetal cardiovascular arteries form independently of the VOC and of each other along the midline, and converge at the VOC to forge the OUA connection. Thus, the VOC is a fulcrum around with the major arterial vessels unite to form a patent OUA connection. While such stereotypically fixed vascular branchpoints have been described in zebrafish (Weinstein, 1999), to the best of our knowledge, the VOC is the first example of such a fixed arterial branchpoint in mammals.

We had previously suggested that the omphalomesenteric artery was an extension of the VOC (Daane and Downs, 2011). However, in FGFR1-inhibited scenarios, loss of the VOC had no affect on formation of the omphalomesenteric artery. Thus, the omphalomesenteric artery forms independently of the VOC. These data also suggested the sequence by which each major arterial vessel joined the VOC. The omphalomesenteric artery, positioned just anterior to the VOC, was the first to join the confluence. The umbilical artery came next, followed by the paired fetal dorsal aortae. In this way, the mouse confluence is similar to that which we observed in humans, where the omphalomesenteric and umbilical arteries unite at the VOC in advance of joining to the dorsal aortae (Fig. 6**J, K**).

During the first phase of remodeling, the VOC recurved over the hindgut to form the medial umbilical roots (Fig. 7**E**). The medial umbilical roots were present but foreshortened in T^{C}/T^{+} heterozygotes. Reduced VOC recurvature over the hindgut in these mutants was probably due to prior repositioning the allantoic-yolk sac junction and VOC within the embryo, obviating the need for VOC remodeling. In T^{C}/T^{C} homozygous mutants, the VOC formed, but was not properly placed at the midline, resulting in failure to forge an OUA connection and failure in turn to form the medial umbilical roots. While fate mapping was not carried out, these data are consistent with the possibility that the VOC is the source of the medial umbilical roots, whose origin is hitherto unknown.

In the second remodeling phase (Fig. 7**F**), the medial umbilical roots begin to regress, and are overtaken by the lateral umbilical roots which sprout from the aorta and are continuous with the developing hindlimb plexus. If the medial roots are not placed at the correct axial level in the previous step, the lateral roots will also be misplaced, thereby compromising formation of the common iliac arteries (Gest and Carron, 2003) that divide the flow of blood from the aorta into each hindlimb. As described in the next section, misplacement of the medial and lateral umbilical roots may compromise posterior development of the fetus.

4.2. Defects in the OUA connection are associated with posterior abnormalities in the fetus

Thus, the ACD and VOC, neither of which, at present, has status in standard anatomical atlases, work together to coordinate successful formation of the fetal-placental vascular confluence. Genesis of this connection involves a series of well-orchestrated steps, where each individual event in turn affects the next one. While we have not shown that the aberrantly forged OUA connection is actually the cause of associated posterior defects in T^{C}/T^{+} heterozygotes, this is likely to be the case, as the blood supply to the posterior limbs and gastrointestinal tract is affected in these mutants (Inman and Downs, 2006b; Searle, 1966). While the vasculature has not been examined in known mouse models for sirenomelia, some mice mutant for *T* exhibit sirenomelialike posterior birth defects (Gluecksohn-Schoenheimer and Dunn, 1945). Other models of sirenomelia exhibit a reduction in T (Abu-Abed et al., 2001; Sakai et al., 2001; Zakin et al., 2005). Moreover, in sirenomelia, the medial umbilical roots are missing (Garrido-Allepuz et al., 2012; Zakin et al., 2005) without concomitant effects on cell death (Zakin et al., 2005), similar to our findings in T^{C}/T^{C} homozygous mutants. Clinically in humans, posterior defects encompassing the hindlimbs in the orphan disease, sirenomelia, are associated with axial misplacement of the umbilical artery to the aorta (Stevenson et al., 1986); affected individuals typically die immediately after birth. This is reminiscent of the sirenomelia (*srn*/*srn*) mouse mutant (Hoornbeek, 1970) in which the left and right umbilical arteries merge to form a single one that is anteriorly misplaced along the midline aorta (Schreiner and Hoornbeek, 1973). Unfortunately, the status of T is not known in these mutants, and the last known study to use the *srn* mouse strain was published about 35 years ago (Orr et al., 1982).

Foreshortening of the umbilical roots as observed in the T^{C}/T^{+} heterozygotes may have other parallels in humans. In humans, a shortened umbilical cord causes the fetus to be tethered too closely to the placenta and can lead to often-severe abdominal wall defects and axial growth retardation due to restrictive fetal position (Stevenson and Hall, 2006). Short cords have been associated with axial defects, leading to various forms of fetal distress and poor prognosis (Stevenson and Hall, 2006). A better understanding of the umbilical cord's ontogeny may lead to improved identification and clinical management of pregnancies at risk of such complications.

Together, these data provide strong evidence that defects in patterning the fetal-placental arterial connection both along the midline and in the VOC itself lead to severe posterior abnormalities in the fetus, and may include sirenomelia and the short-cord spectrum.

4.3. The primitive streak organizes the arterial vasculature

In non-mammalian species, including birds, the notochord may induce and/or appropriately pattern the dorsal aortae with respect to the midline (Hogan and Bautch, 2004). However, there is no evidence that the notochord is required in mammals for vascular patterning (Hogan and Bautch, 2004). Perhaps this is because the primitive streak, from which the notochord is derived, is required for mesoderm formation. Thus, as streak abnormalities can lead to loss of the circulatory system and fetal death that would preclude vascular analysis, T^C mutants may represent a valuable resource for understanding vascular patterning along the midline. In T^C/T^C mutants, the embryonic primitive streak and notochord were present, and persisted long enough, i.e., through 6–9s, to ensure adequate production and patterning of mesoderm into the dorsal aortae and omphalomesenteric artery so that they could be studied. By contrast, the posterior component of the streak, the ACD, did not extend into the allantois in T^C/T^C homozygous mutants, resulting in mispatterning of the allantoic angioblasts and the umbilical artery. Given that the ACD was present in the T^C/T^+ heterozygotes and umbilical patterning was normal, but absent in the T^C/T^C mutants concomitant with abnormal umbilical patterning, we find this to be strong evidence that the primitive streak is required for patterning the major axial arterial vessels in mammals as in other vertebrates.

4.4. Conclusions and future prospects

In light of our results, abnormal formation of the OUA connection should be re-examined in the many mouse models in which mutations affect development of the umbilical component of the placenta (Inman and Downs, 2007). Allantoic defects are often associated with abnormalities in the body axis and organogenesis in the posterior region of the embryo (Inman and Downs, 2007). From a translational point of view, the obstetrics and pediatric literature is full of anecdotal descriptions of vascular disruptions between the fetus and its mother. The outcome of the present study provides new insight into the earliest steps of fetalplacental patency. We anticipate that these findings will alert scientists and clinicians to seek out the VOC branchpoint as a key factor in interpreting vascular defects in hundreds of mouse models of disease that involve the placenta, as well as identify the VOC as a potential risk factor in neonatal vascular defects that merits further screening, evaluation, and ultimately, therapeutic intervention.

Acknowledgments

The authors are grateful to Ben August of the UW-Madison Medical School Electron Microscope Facility for help with plastic histology, to the Louisiana State University Health Sciences Center for making the DREM project available on the public domain for educational and research purposes, and to Dr. C. Schreiner for helpful discussions concerning the current status of the *srn* mouse mutant. This work was supported by research funding from the March of Dimes (1-FY06-355, 1-FY09-511, and 6-FY12-271 to K.M.D.); the National Institutes of Health (R01 HD042706 and RO1 HD079481 to K.M.D; T32 HL07899 and NOT-OD-11-086 to A.D.W.; R25 GM083252 and T32 HD041921 to A.M.R; RO1 HD37811 for DREM project); the National Science Foundation (Pre-doctoral Fellowship to M.M.M. DGE-0718123 and DGE-1256259); the Science & Medicine Graduate Research Scholars Program (Advanced Opportunity Fellowship to A.M.R.) and the Deutsche Forschungsgemeinschaft (Vi151/8-1 to C.V). Support was also provided by the Graduate School and the Office of the Vice Chancellor for Research and Graduate Education at the University of Wisconsin-Madison with funding from the Wisconsin Alumni Research Foundation (to M.M.M).

References

Abu-Abed S, Dollé P, Metzger D, Beckett B, Chambon P. The retinoic acidmetabolizing enzyme, CYP26A1, is essential for normal hindbrain patterning, vertebral identity, and development of posterior structures. Genes Dev. 2001; 15:226–240. [PubMed: 11157778]

Arora R, Papaioannou VE. The murine allantois: a model system for the study of blood vessel formation. Blood. 2012; 120:2562–2572. [PubMed: 22855605]

Beddington RSP. Induction of a second neural axis by the mouse node. Development. 1994; 120:613–620. [PubMed: 8162859]

Blum M, Andre P, Muders K, Schweickert A, Fischer A, Bitzer E, Bogusch S, Beyer T, van Straaten HW, Viebahn C. Ciliation and gene expression distinguish between node and posterior notochord in the mammalian embryo. Differ Res Biol Divers. 2007; 75:133–146.

Bonnevie K. New facts on mesoderm formation and proamnion derivatives in the normal mouse embryo. J Morphol. 1950; 86:495–546. [PubMed: 24537610]

Böttcher RT, Niehrs C. Fibroblast growth factor signaling during early vertebrate development. Endocr Rev. 2005; 26:63–77. [PubMed: 15689573]

Chesley P. Development of the short-tailed mutant in the house mouse. J Exp Zool. 1935; 70:429–459.

Ciruna B, Rossant J. FGF signaling regulates mesoderm cell fate specification and morphogenetic movement at the primitive streak. Dev Cell. 2001; 1:37–49. [PubMed: 11703922]

Cox CM, Poole TJ. Angioblast differentiation is influenced by the local environment: fgf-2 induces angioblasts and patterns vessel formation in the quail embryo. Dev Dyn. 2000; 218:371–382. [PubMed: 10842363]

Daane JM, Downs KM. Hedgehog signaling in the posterior region of the mouse gastrula suggests manifold roles in the fetal-umbilical connection and posterior morphogenesis. Dev Dyn. 2011; 240:2175–2193. [PubMed: 22016185]

Daane JM, Enders AC, Downs KM. Mesothelium of the murine allantois exhibits distinct regional properties. J Morphol. 2011; 272:536–556. [PubMed: 21284019]

Deng CX, Wynshaw-Boris A, Shen MM, Daugherty C, Ornitz DM, Leder P. Murine FGFR-1 is required for early postimplantation growth and axial organization. Genes Dev. 1994; 8:3045–3057. [PubMed: 8001823]

Dorey K, Amaya E. FGF signalling: diverse roles during early vertebrate embryogenesis. Development. 2010; 137:3731–3742. [PubMed: 20978071]

Downs KM. In vitro methods for studying vascularization of the murine allantois and allantoic union with the chorion. Methods Mol Med. 2006; 121:241–272. [PubMed: 16251748]

Downs KM. Systematic localization of Oct-3/4 to the gastrulating mouse conceptus suggests manifold roles in mammalian development. Dev Dyn. 2008; 237:464–475. [PubMed: 18213575]

Downs KM. The enigmatic primitive streak: prevailing notions and challenges concerning the body axis of mammals. Bioessay : News Rev Mol Cell Dev Biol. 2009; 31:892–902.

Downs KM, Davies T. Staging of gastrulating mouse embryos by morphological landmarks in the dissecting microscope. Development. 1993; 118:1255–1266. [PubMed: 8269852]

Downs KM, Gifford S, Blahnik M, Gardner RL. Vascularization in the murine allantois occurs by vasculogenesis without accompanying erythropoiesis. Development. 1998; 125:4507–4520. [PubMed: 9778509]

Downs KM, Inman KE, Jin DX, Enders AC. The Allantoic Core Domain: new insights into development of the murine allantois and its relation to the primitive streak. Dev Dyn. 2009; 238:532–553. [PubMed: 19191225]

Dumont DJ, Fong GH, Puri MC, Gradwohl G, Alitalo K, Breitman ML. Vascularization of the mouse embryo: a study of flk-1, tek, tie, and vascular endothelial growth factor expression during development. Dev Dyn. 1995; 203:80–92. [PubMed: 7647376]

Garrido-Allepuz C, Gonzalez-Lamuno D, Ros MA. Sirenomelia phenotype in bmp7;shh compound mutants: a novel experimental model for studies of caudal body malformations. PLoS One. 2012; 7:e44962. [PubMed: 23028704]

Gest TR, Carron MA. Embryonic origin of the caudal mesenteric artery in the mouse. Anat Rec. 2003; 271A:192–201.

Gluecksohn-Schoenheimer S, Dunn LC. Sirens, aprosopi and intestinal abnormalities in the house mouse. Anat Rec. 1945; 92:201–213.

Hassoun R, Schwartz P, Feistel K, Blum M, Viebahn C. Axial differentiation and early gastrulation stages of the pig embryo. Differ Res Biol Divers. 2009; 78:301–311.

Herrmann BG. Expression pattern of the Brachyury gene in whole-mount T^{Wis}/T^{Wis} mutant embryos. Development. 1991; 113:913–917. [PubMed: 1821859]

Herrmann BG, Labeit S, Poustka A, King TR, Lehrach H. Cloning of the T gene required in mesoderm formation in the mouse. Nature. 1990; 343:617–622. [PubMed: 2154694]

Hogan KA, Bautch VL. Blood vessel patterning at the embryonic midline. Curr Top Dev Biol. 2004; 62:55–85. [PubMed: 15522739]

Hoornbeek FK. A gene producing symmelia in the mouse. Teratology. 1970; 3:7–10. [PubMed: 5418338]

Ingalls, NW. A Human Embryo at the Beginning of Segmentation, with Special Reference to the Vascular System No 52. Carnegie Institution of Washington Publication; 1920.

Inman K, Downs KM. Localization of Brachyury (T) in embryonic and extraembryonic tissues during mouse gastrulation. Gene Exp Patterns. 2006a; 6:783–793.

Inman KE, Downs KM. Brachyury is required for elongation and vasculogenesis in the murine allantois. Development. 2006b; 133:2947–2959. [PubMed: 16835439]

Inman KE, Downs KM. The murine allantois: emerging paradigms in development of the mammalian umbilical cord and its relation to the fetus. Genesis. 2007; 45:237–258. [PubMed: 17440924]

Lawson KA, Meneses JJ, Pedersen RA. Clonal analysis of epiblast fate during germ layer formation in the mouse embryo. Development. 1991; 113:891–911. [PubMed: 1821858]

Lee SH, Schloss DJ, Swain JL. Maintenance of vascular integrity in the embryo requires signaling through the fibroblast growth factor receptor. J Biol Chem. 2000; 275:33679–33687. [PubMed: 10930413]

Lin X. Functions of heparan sulfate proteoglycans in cell signaling during development. Development. 2004; 131:6009–6021. [PubMed: 15563523]

Magnusson P, Rolny C, Jakobsson L, Wikner C, Wu Y, Hicklin DJ, Claesson-Welsh L. Deregulation of Flk-1/vascular endothelial growth factor receptor-2 in fibroblast growth factor receptor-1-deficient vascular stem cell development. J Cell Sci. 2004; 117:1513–1523. [PubMed: 15020678]

McGrath KE, Koniski AD, Malik J, Palis J. Circulation is established in a stepwise pattern in the mammalian embryo. Blood. 2003; 101:1669–1676. [PubMed: 12406884]

Mikedis MM, Downs KM. STELLA-positive subregions of the primitive streak contribute to posterior tissues of the mouse gastrula. Dev Biol. 2012; 363:201–218. [PubMed: 22019303]

Mikedis MM, Downs KM. Widespread but tissue-specific patterns of interferon-induced transmembrane protein 3 (IFITM3, FRAGILIS, MIL-1) in the mouse gastrula. Gene Expr Patterns. 2013; 13:225–239. [PubMed: 23639725]

Mikedis MM, Downs KM. Mouse primordial germ cells: a reappraisal. Int Rev Cell Mol Biol. 2014; 309:1–57. [PubMed: 24529721]

Mohammadi M, Froum S, Hamby JM, Schroeder MC, Panek RL, Lu GH, Eliseenkova AV, Green D, Schlessinger J, Hubbard SR. Crystal structure of an angiogenesis inhibitor bound to the FGF receptor tyrosine kinase domain. EMBO J. 1998; 17:5896–5904. [PubMed: 9774334]

Niwa H, Miyazaki J, Smith AG. Quantitative expression of Oct-3/4 defines differentiation, dedifferentiation or self-renewal of ES cells. Nat Genet. 2000; 24:372–376. [PubMed: 10742100]

Oki S, Kitajima K, Meno C. Dissecting the role of Fgf signaling during gastrulation and left-right axis formation in mouse embryos using chemical inhibitors. Dev Dyn. 2010; 239:1768–1778. [PubMed: 20503372]

O'Rahilly R, Müller F. Developmental stages in human embryos: revised and new measurements. Cells Tissues Organs. 2010; 192:73–84. [PubMed: 20185898]

Orr BY, Long SY, Steffek AJ. Craniofacial, caudal, and visceral anomalies associated with mutant sirenomelic mice. Teratology. 1982; 26:311–317. [PubMed: 6891838]

Sakai Y, Meno C, Fujii H, Nishino J, Shiratori H, Saijoh Y, Rossant J, Hamada H. The retinoic acid-inactivating enzyme CYP26 is essential for establishing an uneven distribution of retinoic acid along the anterio-posterior axis within the mouse embryo. Genes Dev. 2001; 15:213–225. [PubMed: 11157777]

Schreiner CA, Hoornbeek FK. Developmental aspects of sirenomelia in the mouse. J Morphol. 1973; 141:345–358. [PubMed: 4753445]

Seano G, Chiaverina G, Gagliardi PA, di Blasio L, Puliafito A, Bouvard C, Sessa R, Tarone G, Sorokin L, Helley D, Jain RK, Serini G, Bussolino F, Primo L. Endothelial podosome rosettes regulate vascular branching in tumour angiogenesis. Nat Cell Biol. 2014; 16(931–941):931–938. [PubMed: 25218639]

Searle AG. Curtailed, a new dominant T-allele in the house mouse. Genet Res. 1966; 7:86. [PubMed: 5906493]

Stevenson, RE., Hall, JG. Human Malformations and Related Anomalies. Oxford University Press; 2006.

Stevenson RE, Jones KL, Phelan MC, Jones MC, Barr M, Clericuzio C, Harley RA, Benirschke K. Vascular Steal: the pathogenetic mechanism producing sirenomelia and associated defects of the viscera and soft tissue. Pediatrics. 1986; 78:451–457. [PubMed: 3748679]

Stott D, Kispert A, Herrmann BG. Rescue of the tail defect of Brachyury mice. Genes Dev. 1992; 7:197–203.

Walls JR, Coultas L, Rossant J, Henkelman RM. Three-dimensional analysis of vascular development in the mouse embryo. PLoS One. 2008; 3:e2853. [PubMed: 18682734]

Watson ED, Cross JC. Development of structures and transport functions in the mouse placenta. Physiology. 2005; 20:180–193. [PubMed: 15888575]

Weinstein BM. What guides early embryonic blood vessel formation? Dev Dyn. 1999; 215:2–11. [PubMed: 10340752]

Yamaguchi TP, Harpal K, Henkemeyer M, Rossant J. *fgfr-1* is required for embryonic growth and mesodermal patterning during mouse gastrulation. Genes Dev. 1994; 8:3032–3044. [PubMed: 8001822]

Zakin L, Reversade B, Kuroda H, Lyons KM, De Robertis EM. Sirenomelia in Bmp7 and Tsg compound mutant mice: requirement for Bmp signaling in the development of ventral posterior mesoderm. Development. 2005; 132:2489–2499. [PubMed: 15843411]

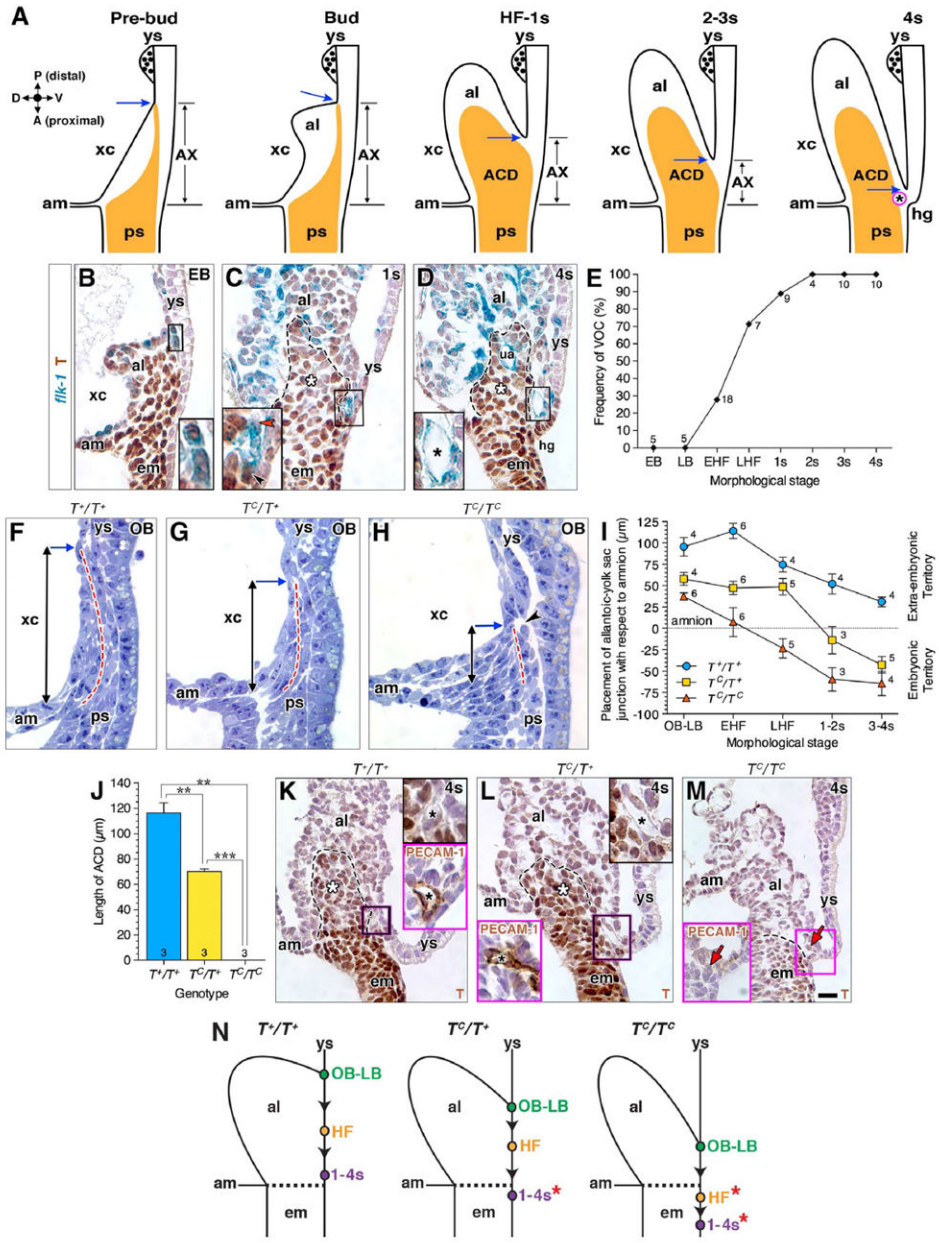

Fig. 1. Positioning the allantoic-yolk sac junction and vessel of confluence requires *T*

Unless otherwise indicated, histological sections in this (B-D, K-M: paraffin wax preparation; F-H: plastic preparation) and all subsequent figures are mid-sagittal with orientation as depicted by compass in A (A, anterior (proximal); D, dorsal; P, posterior (distal); V, ventral). **(A)** Schematic diagram through the mid-sagittal plane of the posterior embryonic-extraembryonic interface over time; data are from previous reports (see text) regarding the allantois-associated visceral endoderm (AX), the primitive streak's extraembryonic extension/ACD (orange), and the VOC (magenta; black asterisk). The posterior limit of the primitive streak coincides with the posterior limit of the allantoic bud's ventral connection to the single layer of yolk sac mesoderm, called here the "allantoic-yolk sac junction" (blue arrow). (**B-D**) Genesis of the VOC and localization of T in the *flk-1: lacZ*

reporter mouse strain; black dashed lines outline ACD (C, D, white asterisk). Insets are enlarged box regions in main panels. (B) T-positive angioblasts clustering at the allantoic-yolk sac junction; (C) a mixture of T-positive angioblasts (black arrowhead) and T-negative endothelializing angioblasts (red arrowhead) as the cluster matures; (D) the fully mature T-negative VOC (black asterisk). (**E**) Graph showing that the appearance of the endothelialized VOC begins at the early headfold stage, and is invariably present by 2s. Sample sizes are indicated at each data point. (**F-H**) Comparison, amongst T^C littermates, of the primitive streak's extension into the extraembryonic region (dashed red line); vertical arrows indicate the distance of this extension measured from the amnion to the allantoic-yolk sac junction (blue arrow). Arrowhead (H) indicates that the extraembryonic streak may be fragmenting. (**I**) Placement of the allantoic-yolk junction decreases over time amongst all T^C genotypes. The mean distance ± SEM (error bars) measured vertically from the amnion, shown in (F-H) (y=0, embryonic-extraembryonic boundary); sample sizes per stage and genotype are indicated for each data point. (**J**) Length of ACD, depicted as mean ± SEM (error bars) with sample sizes indicated at the base of each bar; asterisk, significant *P*-value (Student *t*-Test: T^+/T^+ vs T^C/T^+, P=0.0051; T^+/T^+ vs T^C/T^C, P=0.0047; T^C/T^+ vs T^C/T^C, P=0.0009). (**K-M**) T immunostaining in main panels; upper right insets (K, L) are enlarged from the boxed region of the main panel, showing the VOC (black asterisk). Magenta-boxed insets (K-M) show PECAM-1 immunostaining of mid-sagittal sections through the VOC (K, L), or where the VOC should be, but is missing (red arrow, M). Black dashed lines outline the posteriormost extension of the primitive streak, which extends into the allantois (ACD, white asterisk) in K and L, but is limited to the embryo in M. (**N**) Schematic representation of how placement of the allantoic-yolk sac junction (color-filled dots along yolk sac) drops (arrowheads) anteriorly (proximally) over time in each genotype. Dashed line indicates embryonic-extraembryonic boundary, red asterisk highlights aberrant embryonic placement of the junction in the T^C/T^+ and T^C/T^C mutants, also indicated in (I). Scale bar (M): 10 μm (K, L magenta insets); 18 μm (B-D, F-*H, K, L*, M magenta inset); 25 μm (M). al, allantois; am, amnion; em, embryo; hg, hindgut; ps, primitive streak; ua, umbilical artery; xc, exocoelomic cavity; ys, yolk sac.

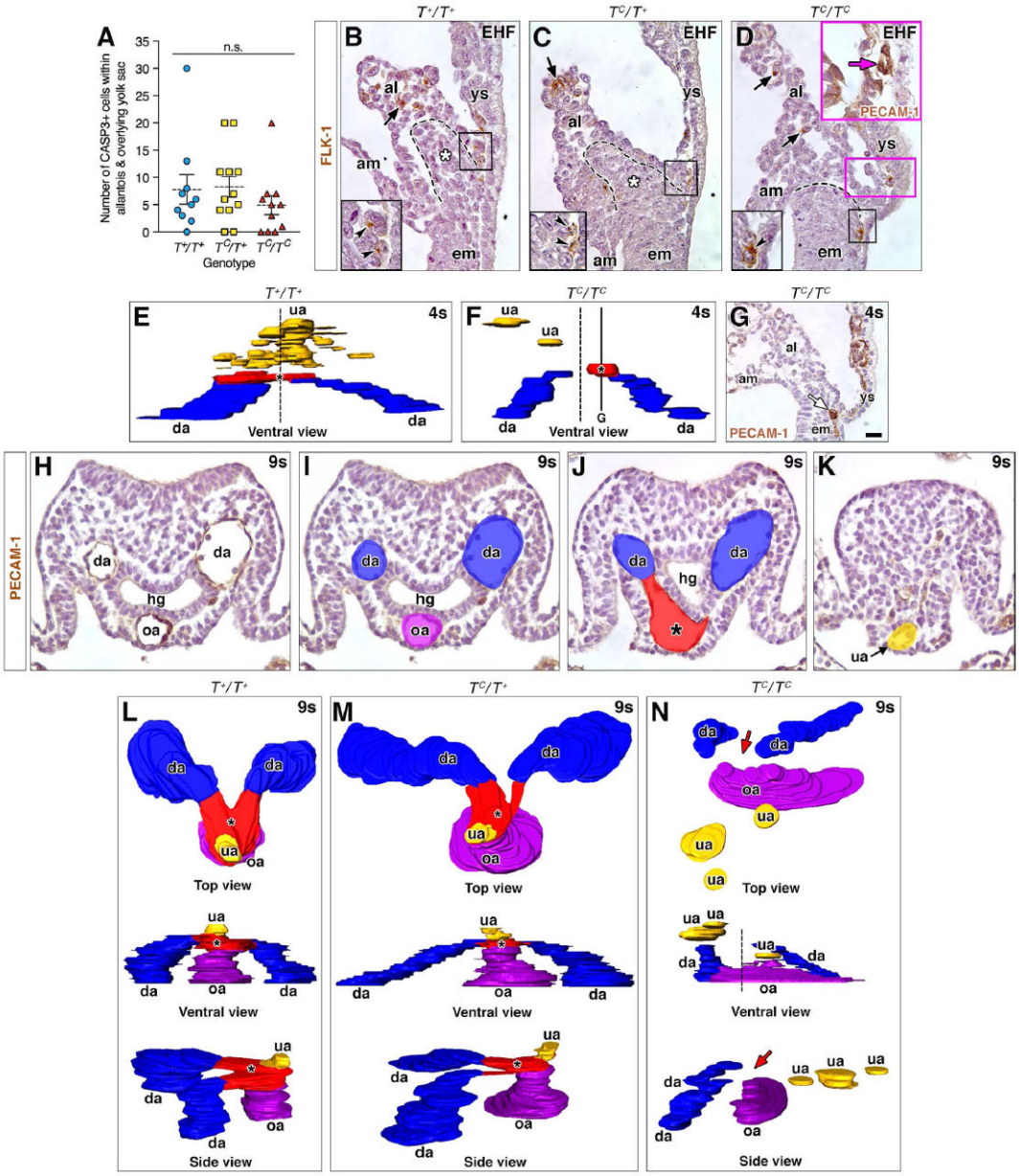

Fig. 2. Placement of the VOC, umbilical artery, and OUA connection is dose-dependent on *T*

(A) Dot-box plot of CASP3+ cells in allantois and overlying yolk sac (EB-6s stages); means (dashed line), SEM (error bars); n.s., not significant (Student *t*-Test; T^{+}/T^{+} vs T^{C}/T^{+}, P=0.8912; T^{+}/T^{+} vs T^{C}/T^{C}, P=0.3714; T^{C}/T^{+} vs T^{C}/T^{C}, P=0.2134). (**B-D**) Immunostaining for FLK-1 amongst T^{C} genotypes. Black boxed insets, lower left: enlarged prospective VOC of black-boxed region in main panels. Black arrows (main panels) and arrowheads (insets): correctly patterned FLK-1 angioblasts within distal allantois and prospective VOC. Dashed lines, posteriormost extension of primitive streak (B-D); white asterisk, ACD (B, C). Magenta inset (D): a misplaced PECAM-1-positive (magenta arrow) vessel within the yolk sac near its junction with the allantois, the region of which is indicated by the magenta box in the main panel (see text). (**E, F**) 3D models (frontal ventral views) reconstructed from

PECAM-1-immunostained nascent arterial vessels at the posterior embryonic-extraembryonic interface; dashed vertical line (E, F) marks the axial midline. Color key: blue, dorsal aortae (da); red, VOC (asterisk); yellow, umbilical artery (ua). (**G**) T^C/T^C mutant specimen immunostained for PECAM-1, sagittal section, lateral to the midline, equivalent to the solid horizontal line in F. White arrow indicates a vessel forming at the allantoic-yolk sac junction off the midline. (**H-K**) Examples of tissue sections used for the 3D reconstructions in (L-N). (H) PECAM-1-immunostained transverse section showing the paired da on either side of the hindgut (hg), and the omphalomesenteric artery (oa) at the ventral midline. (I-K) Colorized transverse sections from the level of the oa (H, I) and proceeding posteriorly (distally), to capture the VOC (J) and ua (K). All reconstructed sections were PECAM-1 immunostained. (**L-N**) Top, ventral (frontal) and side views (posterior, right) of the OUA connection in all three *T* genotypes, colored as described above with addition of purple for the oa. Red arrows (N) indicate missing OUA connection; vertical dashed line indicates the axial midline and the site where the VOC (red, located off center) should be located. Scale bar (G): 10 μm (D magenta inset); 20 μm (B-D, H-K), 25 μm (G). al, allantois; am, amnion; em, embryo; ys, yolk sac.

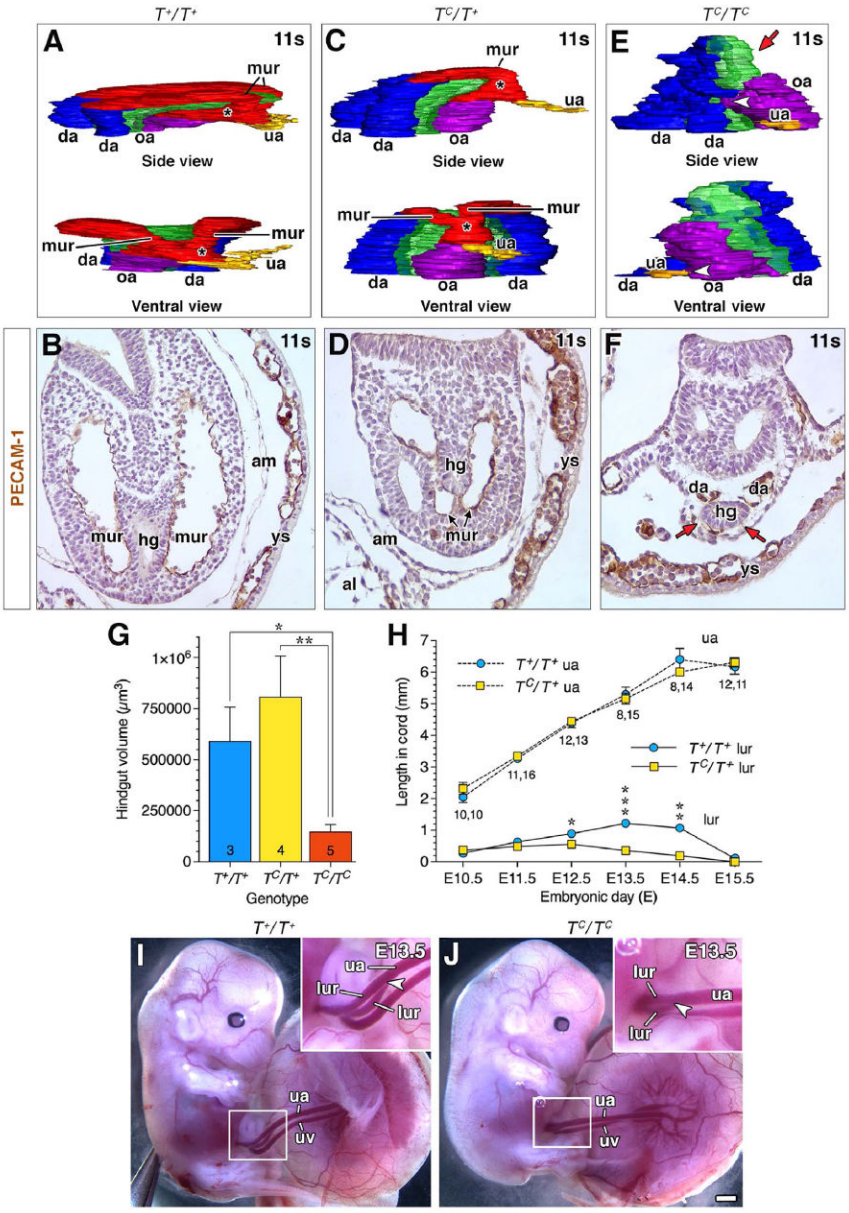

Fig. 3. Downstream consequences on vascular remodeling of the OUA connection as a result of earlier misplacement of the VOC

(A, C, E) 3D models reconstructed from PECAM-1-immunostained arterial vessels and associated hindgut at the posterior embryonic-extraembryonic interface in T^C littermates during vascular remodeling of the OUA connection (11s stage). Color key as described in Fig. 2, with the addition of green for the hindgut. mur, medial umbilical roots, missing in panel E (red arrow); white arrowhead (E), partial arterial union. Side views, posterior to the right. See text for further details. (**B, D, F**) Transverse PECAM-1-immunostained histological sections taken at the same level in each of the three T genotypes to illustrate the fully extended mur in the wildtype (B), reduced mur in the heterozygotes (D), and the absence of the mur (red arrows) in the homozygotes (F). (G) Volume of hindgut (7–10s) in T^C littermates, depicted as mean ± SEM (error bars) with sample sizes indicated at the base

of each bar; asterisk, significant *P*-values (Student *t*-Tests; $T+/T^{+}$ vs T^{C}/T^{C}, P=0.0078; T^{C}/T^{+} vs T^{C}/T^{C}, P=0.0005). (H) Average length of umbilical artery (upper data points) and lateral umbilical roots (lur; lower data points) as a function of nominal days postcoitum ("embryonic day, E"). Data plotted as mean ± SEM (error bars) with sample sizes for each stage and genotype (T^{+}/T^{+}, T^{C}/T^{+}) displayed below each data point; asterisk, significant *P*-values (Student *t*-Tests; E12.5 T^{+}/T^{+} lur vs T^{C}/T^{+} lur, P=0.0122; E13.5 T^{+}/T^{+} lur vs T^{C}/T^{+} lur, P=0.0002; E14.5 T^{+}/T^{+} lur vs T^{C}/T^{+} lur, P=0.0062). (I, J) Fetalplacental unit, ~E13.5, proximal portion of umbilical cord, i.e. closest to the fetus, is boxed and enlarged in insets. Arrowheads indicate the posterior extent of lateral umbilical roots in the umbilical cord. Scale bar (J): 22 μm (B, D, F); 1 mm (I, J). uv, umbilical vein.

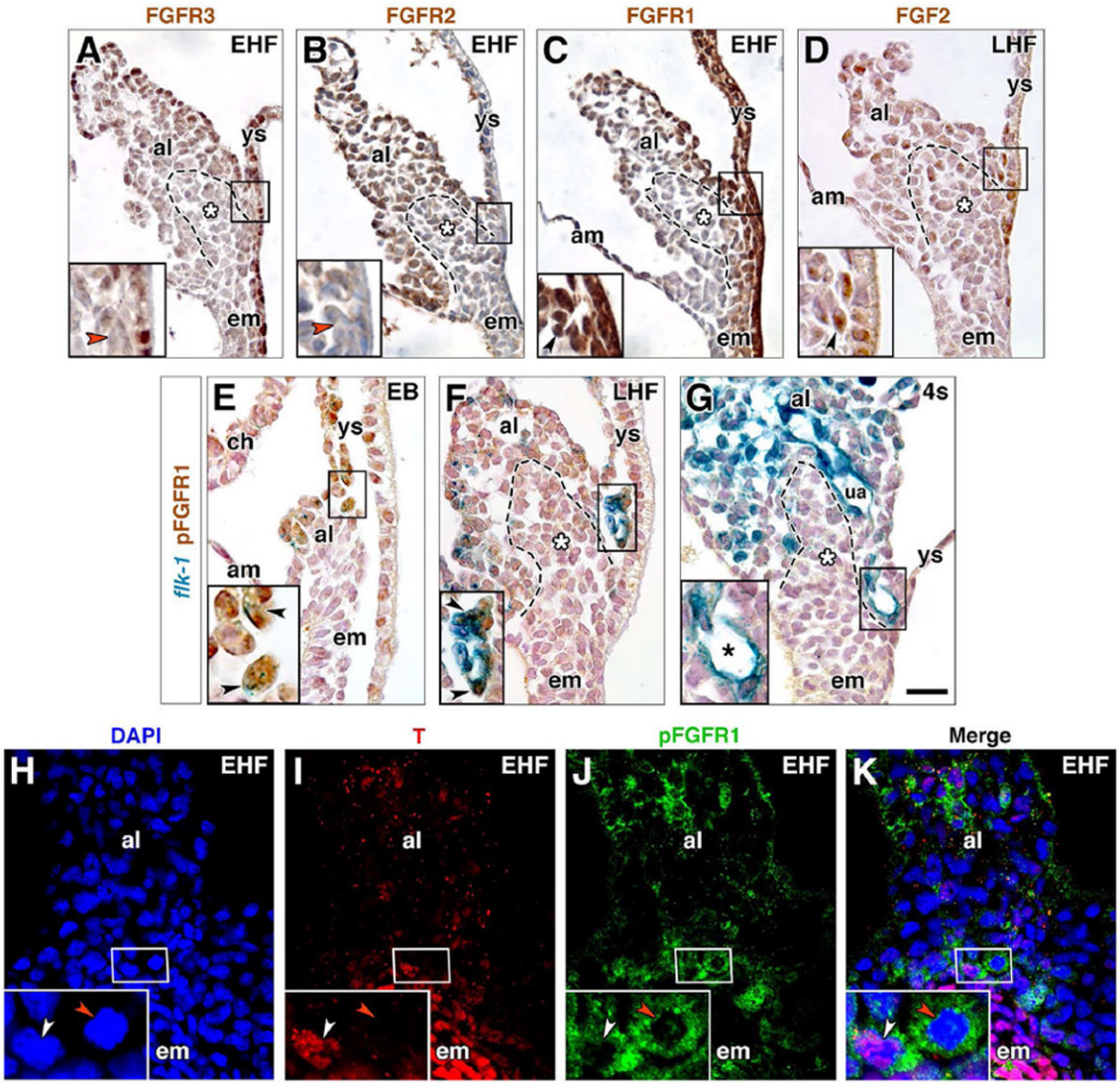

Fig. 4. Localization of FGF members within the nascent VOC

(**A-G**) Immunostaining for FGFR3 (A), FGFR2 (B), FGFR1 (C), FGF2 (D), all at the headfold stages, and pFGFR1 (E-G) in EB through 4s stage *flk-1: lacZ* reporter specimens. Boxed region in main panels is the prospective VOC (A-E) or endothelialized VOC (F, G) region, enlarged in insets, lower left. Dashed outline, posteriormost (distalmost) extension of the primitive streak, and white asterisk, ACD (A-D, F, G). Red arrowheads (A, B), FGFR-3- and FGFR-2-negative cells. Black arrowhead (C), FGFR1-positive rosette. Black arrowhead (D), FGF2-positive cell. Black arrowheads (E, F), *flk-1*-positive/pFGFR1-positive angioblasts. Black asterisk (G), *flk-1*-positive/pFGFR1-negative mature VOC. (**H-K**) EHF stage, frontal (ventral) optical section through ventral allantoic and embryonic tissue stained with DAPI (H), T (I), pFGFR1 (J); channels merged (K). Insets are enlargements of prospective VOC, boxed in main panels. White arrowhead, T-positive/pFGFR1-positive angioblast; red arrowhead, pFGFR1-positive/T-negative angioblast. Scale bar (G): 20 μm (A-K). al, allantois; am, amnion; ch, chorion; em, embryo; ua, umbilical artery; ys, yolk sac.

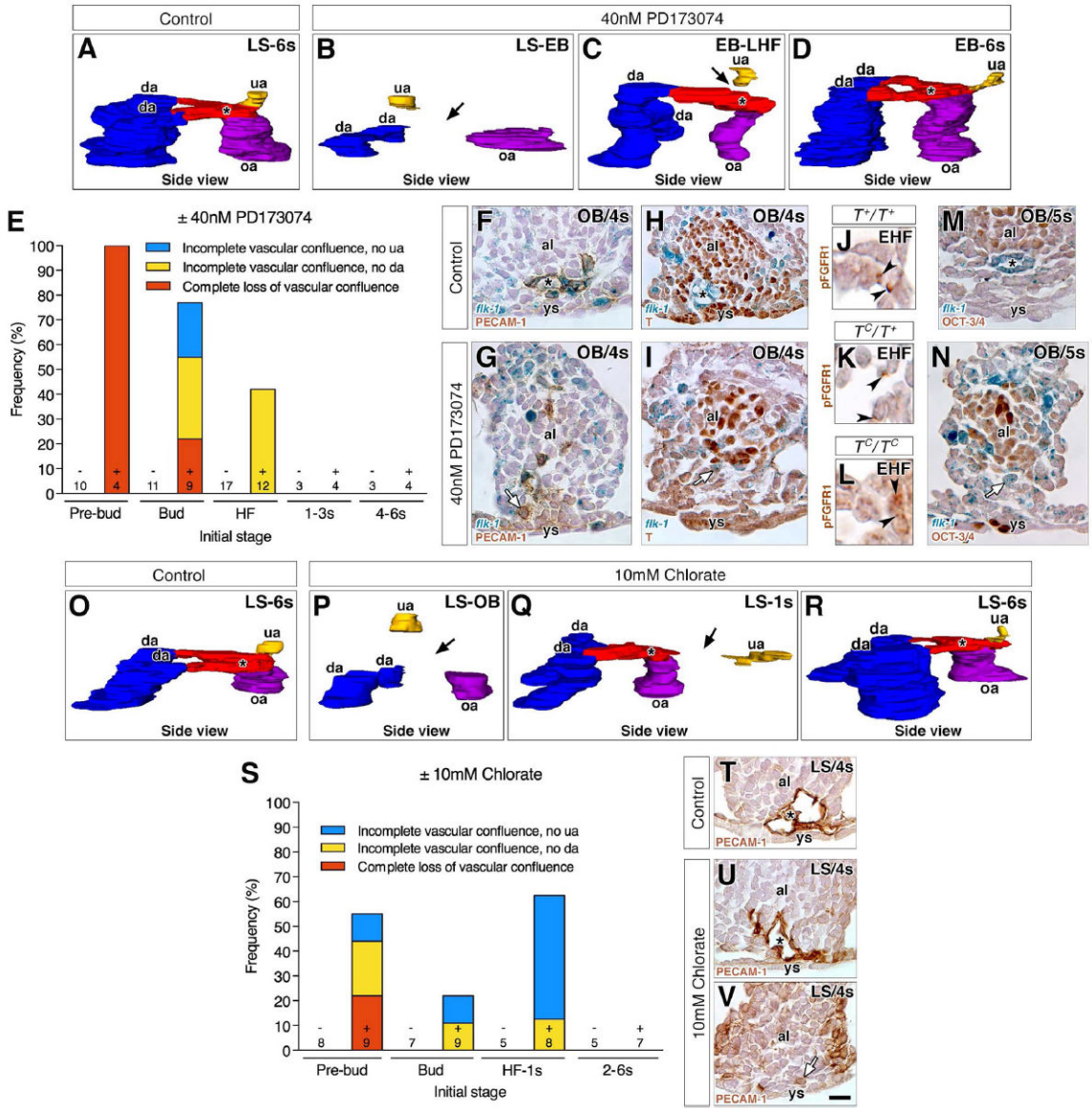

Fig. 5. Stage-specific failure of formation of the vascular confluence in PD173074- or chlorate-treated specimens

"Control" indicates untreated conceptuses that were cultured alongside pharmacologically-treated ones until 7–8s stage. Transverse histological sections (F-I, M, N, T-V) are oriented with ventral toward the bottom. Black asterisk indicates the VOC (A, C, D, F, H, M, O, Q, R, T, U). (**A-D, O-R**) 3D models, in side view (posterior to the right), reconstructed from post-culture PECAM-1-immunostained arterial vessels at the posterior embryonic-extraembryonic interface of control (A, O), PD173074-treated (B-D) or chlorate-treated (P-R) conceptuses (initial stages, upper right). Color key as in Fig. 2. Black arrows indicate missing arterial connections due to loss of the VOC (B, P) or to incomplete branching of the VOC (C, Q). (**E, S**) Frequency of anomalies observed in the vascular confluence in post-culture specimens from PD173074 (E) or chlorate (S) experiments by their initial stage, sample size and group's treatment (± PD173074 or chlorate). (**F, G**) Transverse sections in

the *flk-1: lacZ* reporter showing the PECAM-1-positive endothelialized VOC in the control (F), but non-endothelialized angioblasts in the prospective VOC of PD173074-treated specimens (G, white arrow). (**H, I**) Transverse sections in the *flk-1: lacZ* reporter showing down-regulation of T in the endothelialized control VOC (H) and in nonendothelialized angioblasts of the prospective VOC in PD173074-treated specimens (white arrow) (I). (**J-L**) Histological sections through the prospective VOC showing that pFGFR1 is unaffected in the three T^C genotypes. (**M, N**) Transverse sections in the *flk-1: lacZ* reporter showing down-regulation of OCT-3/4 in the endothelialized VOC of untreated controls (M) and in non-endothelialized angioblasts of the prospective VOC in PD173074-treated specimens (N, white arrow). (**T-V**) Transverse histological sections showing the PECAM-1-positive endothelialized VOC in a control (T) and a chlorate-treated specimen (U), and non-endothelialized angioblasts in the prospective VOC of another chlorate-treated specimen (V, white arrow). Scale bar (V): 6 μm (J-L); 25 μm (F-I, M, N, T-V). al, allantois; da, dorsal aortae; omphalomesenteric artery, oa; umbilical artery; ys, yolk sac.

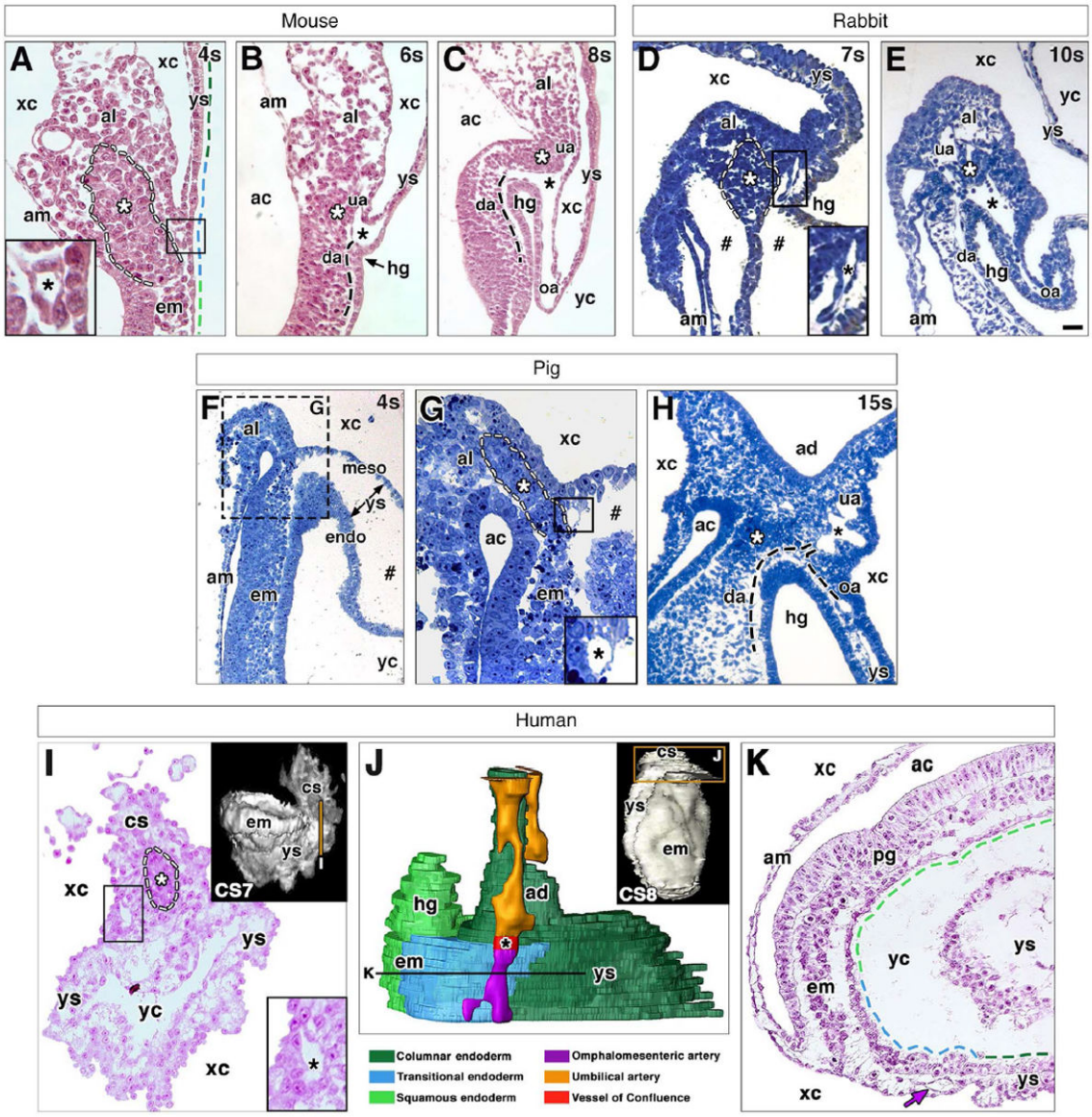

Fig. 6. Conserved features at the posterior embryonic-extraembryonic interface of placental mammals

For all panels: black asterisk (A-E, G-I) indicates VOC; white asterisk (A-E, G-I) and dashed outline (A, D, G, I) indicate dense allantoic core; black dashed line (B, C, H) indicates arterial vessels out of sectional plane; colored dashed lines (A, K) indicate distinct region of visceral endoderm with color key below J; and hash mark (D, F, G) indicates artifactual spaces produced by fixation. (**A-C**) Posterior embryonicextraembryonic interface of a mouse conceptus at the 4s (A), 6s (B) and 8s (C) stage. VOC in A is boxed and enlarged in inset. (**D, E**) Posterior embryonic-extraembryonic interface of a rabbit conceptus at the 7s (D) and 10s (E) stages. VOC in D is boxed and enlarged in inset. (**F-H**) Posterior embryonic-extraembryonic interface of a pig conceptus at the 4s (F, G) and 15s (H) stages. (G) Enlargement of hashed region in F; VOC is boxed in main panel and enlarged in inset. (**I-K**) Posterior embryonic-extraembryonic interface of a human conceptus at Carnegie

stages 7 (I) and 8 (J,K). Volume-rendered models (insets I, J) with transverse sections (I, K) oriented ventral toward the bottom and taken at the level of vertical line (inset I) and horizontal line (J). 3D model (J, color key below), reconstructed from nascent arterial vessels and endoderm (boxed region, inset J). VOC in I is boxed and enlarged in inset. Purple arrow (K) indicates omphalomesenteric artery (oa). Scale bar (E): 20 μm (A, B, I); 40 μm (C, D, G); 90 μm (F); 100 μm (E, H); 300 μm (Insets I, J); 400 μm (K). ac, amniotic cavity; ad, allantoic diverticulum; am, amnion; al, allantois; cs, connecting stalk; da, dorsal aorta; em, embryo; endo, endoderm; hg, hindgut; meso, mesoderm; pg, primitive groove; ua, umbilical artery; xc, exocoelomic cavity; yc, yolk cavity; ys, yolk sac.

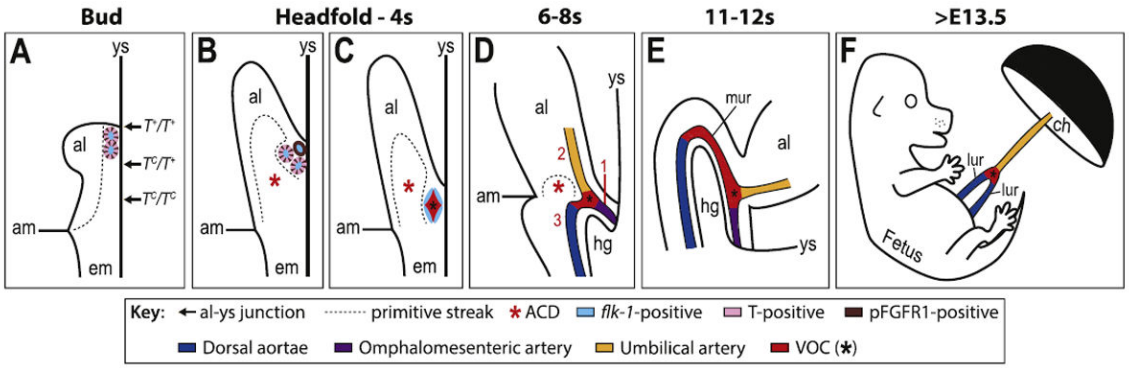

Fig. 7. The primitive streak and VOC collaborate to drive fetal-placental union in the mouse via T and pFGFR1

Schematics in A-C are depicted entirely through the midsagittal plane, while the embryonic component in D, E is slightly lateral, to visualize one of the paired dorsal aortae. (**A**) As the allantoic bud (al) emerges (~E7.25), the T-positive primitive streak (dashed outline) has extended into the extraembryonic region, positioning the allantoic-yolk sac junction (arrows), where prospective VOC angioblasts (colored ovals) exhibit *flk-1* (light blue), pFGFR1 and T (alternating brown and pink, respectively). *T*-dosage, i.e., the number of normal copies of *T* present, regulates extension of the primitive streak and thus, correct axial placement of the allantoic-yolk sac junction according to T^C genotype (arrows) along the anteroposterior axis. (**B**) As the al elongates (~E7.75), the streak (dashed outline) expands into the ACD (red asterisk), where it ensures that the prospective VOC angioblasts (colored ovals), which are now beginning to lose T (pink), are organized to the midline. (**C**) By 2s (~E8.25), angioblasts have endothelialized (light blue flattenedovals) as a result of FGFR1 signaling to form the VOC (red, black asterisk), which now lacks both T (pink) and pFGFR1 (brown). (**D**) By 6–8s (~E8.5), the primitive streak (dashed outline)/ACD (red asterisk) regresses (Downs et al., 2009), and the VOC (red, black asterisk) branches as a result of pFGFR1 signaling to unite, in sequential order (red numbers), the omphalomesenteric artery (purple; 1), umbilical artery (yellow; 2), and dorsal aortae (dark blue; 3) to create the OUA connection. (**E**) Anterior movements during embryonic turning (11s, ~E9.0) cause the VOC (red, black asterisk) to curve around the hindgut (hg), creating the medial umbilical roots (mur). (**F**) Later, during the early-to-mid fetal period (~E13.5), the mur begin to regress, allowing the lateral umbilical roots (lur, dark blue; derived from the dorsal aortae) to assume prominence, connecting to the umbilical artery (yellow) at the VOC branchpoint (red, black asterisk). am, amnion; ch, chorion; em, embryo; ys, yolk sac.